On the predictability of fatigue failure of glassy polymers

de Kanter, D.

Award date:
2006

On the predictability of fatigue failure of glassy polymers

D. de Kanter

MT 06.15
May 9th 2006

Supervisor:
Prof.Dr.Ir. H.E.H. Meijer

Coaches:
Dr.Ir. L.E. Govaert
Ir. R.P.M. Janssen

Eindhoven University of Technology
Department of Mechanical Engineering
Section Material Technology

Abstract

Lifetime predictions are a key-issue in the optimal design of a product in load-bearing applications. In order to perform lifetime predictions, an accurate model of the deformation behaviour of the polymer is needed. Klompen et al. [1, 2] showed a modelling approach capable of lifetime predictions for polymers under static loads. From this work it can be concluded that lifetime of a polymer depends on accumulation of plastic strain. Three parameters have a strong influence on the rate of plastic strain accumulation: stress, temperature and processing history. This approach led to accurate predictions of the lifetime of glassy polymers under static loadings and isothermal conditions. A strength of the model is its implementation of the physical ageing kinetics.

The approach of Klompen et al. is used in this study to predict the deformation behaviour and lifetime of glassy polymers under cyclic loading conditions. An analysis is performed to investigate the influence of stress, temperature and processing history on the fatigue lifetime predictions.

Samenvatting

De levensduur van een product is een belangrijke eis in het ontwerpen van nieuwe producten voor gebruik in aan belasting onderhevige toepassingen. Om uitspraken te kunnen doen over de levensduur van een product, moet het deformatie gedrag van het materiaal kunnen worden gemodelleerd. Klompen et al. [1, 2] tonen een constitutief model dat in staat is levensduur voorspellingen te verrichten voor polymeren onder constante belastingen. Het model voorspelt de levensduur als functie van de geaccumuleerde plastische rek en toont tevens drie parameters die van invloed zijn op de snelheid van accumulatie van plastische rek: spanning, temperatuur en de thermische geschiedenis van het materiaal. Deze aanpak bewijst in staat te zijn van het accuraat voorspellen van de levensduur van glasachtige polymeren onder constante belastingen en isotherme condities. Het model voorspelt tevens de invloed van veroudering van het materiaal op de levensduur.

De aanpak zal in deze studie worden gebruikt om het deformatiegedrag en de levensduur van glasachtige polymeren te voorspellen onder cyclische belasting condities. Tevens zal worden geanalyseerd welke invloed de spanning, temperatuur en thermische geschiedenis van het materiaal hebben op de levensduur.

Contents

Chapter 1

Introduction

A key-issue in the design of new products is their expected lifetime under specified loads. In order to be able to predict this, the deformation behaviour of the product material has to be understood and captured mathematically. For this purpose, several constitutive models have been developed around the world to describe the deformation behaviour of polymers, with varying success.

The development of a constitutive model, accurately describing the deformation behaviour of polymers, is of importance for the engineering world. The combination of constitutive models and finite element packages, can save high costs in product design by cheap and fast, virtual prototyping. In virtual prototyping, in lieu of a physical prototype, products are virtually tested and evaluated on specific characteristics in the design of the product.

Klompen et al. [1–3] reported on a constitutive model developed in Eindhoven. It was shown [1, 2] that the approach is capable of quantitative static loading lifetime predictions. The rationalisation is the lifetime of polymers to be determined by the softening of the material and as in a consequence is governed by the amount of in time accumulated plastic strain. The accumulation of plastic strain proved to be influenced by three parameters: stress, temperature and processing history of the material. The implementation of the constitutive model in a finite element package delivers a design tool that can be used for the virtual prototyping.

In practise, however, products not only have to endure static loadings, but also severe dynamic loadings. Despite all progress made on constitutive modelling, until today a constitutive model describing deformation behaviour under cyclic loading and predicting the fatigue lifetime of polymers, has not yet been reported on. In this study the approach of Klompen et al. [1, 2] is used to predict the lifetime of glassy polymers under cyclic loadings. The applicability of the model are tested for dynamic conditions and the influence of stress, temperature and processing history on the fatigue life are analysed.

Chapter 2

Background

In the last decades a profound progress is made in the development of constitutive models. A number of 3D constitutive models have been developed and validated by several groups around the world, e.g the group of Mary Boyce at MIT [4–6], Paul Buckley in Oxford [7] and our group at the TU/e in Eindhoven [8]. In the past few years important developments were reported by Klompen et al. [1, 2] from the group in Eindhoven. This approach distinguishes itself by the capabilities of the model to predict fast and accurate the time to failure of polymers under static loadings. The model is limited to isothermal conditions and is explained in more detail in this chapter.

2.1 Intrinsic deformation of glassy polymers: phenomenology

The intrinsic deformation behaviour is used for material modelling [8]. The intrinsic behaviour is defined as the true stress-strain behaviour of the material during homogeneous deformation. In figure 2.1(a) a schematic representation is shown of the different intrinsic characteristics that can be witnessed in a compression test.

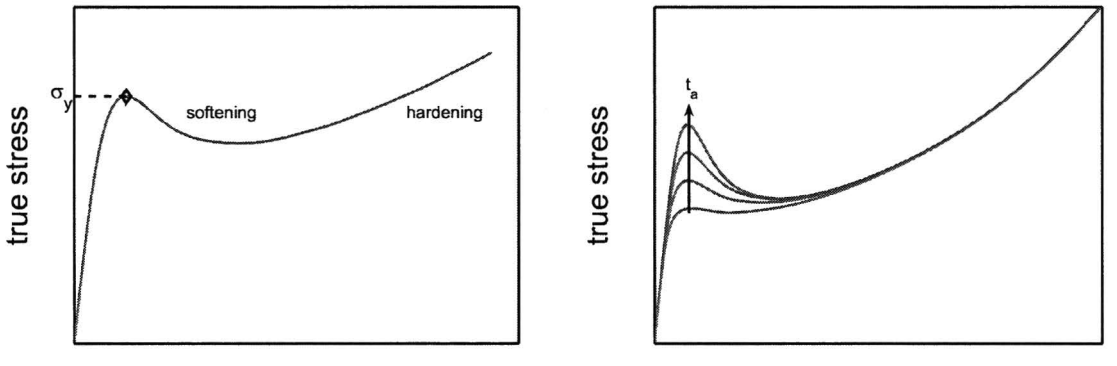

Figure 2.1: *General representation of the intrinsic behaviour under constant strain (σ_y : yield stress)(a). Influence of ageing of the material in time (t_a) on the yield stress (b). Figures adapted from Klompen et al. [9]*

Polymers first show a *linear viscoelastic* relation between stress and strain, where deformation is fully reversible. At increasing strain, deformation becomes *nonlinear viscoelastic* up to the *yield point.* At the yield point the irreversible plastic flow sets in, induced by the stress. The strain build up from this point on is irreversible. With increasing deformation a decrease in stress is observed, *strain softening,* until molecular orientation of the material in the direction of loading increases the stress again, *strain hardening.*

In a tensile test the deformation is not homogeneous and shows localisation phenomena at the moment of softening, that can be observed in the form of moderate localisation (necking or shear banding) and severe localisation (crazing). The localisation phenomena give an indication of the lifetime of the material and are therefore taken as the time-to-failure .

Deformation kinetics

In the deformation behaviour of polymers, two time-depended processes have to be distinguished. The first time depending process relates to the deformation kinetics of the material. The deformation of a material depends on the mobility of the molecular chains or moreover the ability of chain segments to change their conformation by bond rotation. The mobility is impeded by the intramolecular and intermolecular interactions. Stress and temperature stimulate the mobility of the chains and therefore increase the rate of change in conformation.

At the yield point, the stress induced segmental motion of the molecular chain results in a plastic flow rate that exactly balances the applied strain rate. Therefore, the material deforms at the yield point at constant stress and at constant strain rate equal to the prescribed strain rate. The deformation of polycarbonate is rate-dependent as is shown in figure 2.2(a). The relation between the constant strain rate and yield stress is shown in figure 2.2(b).

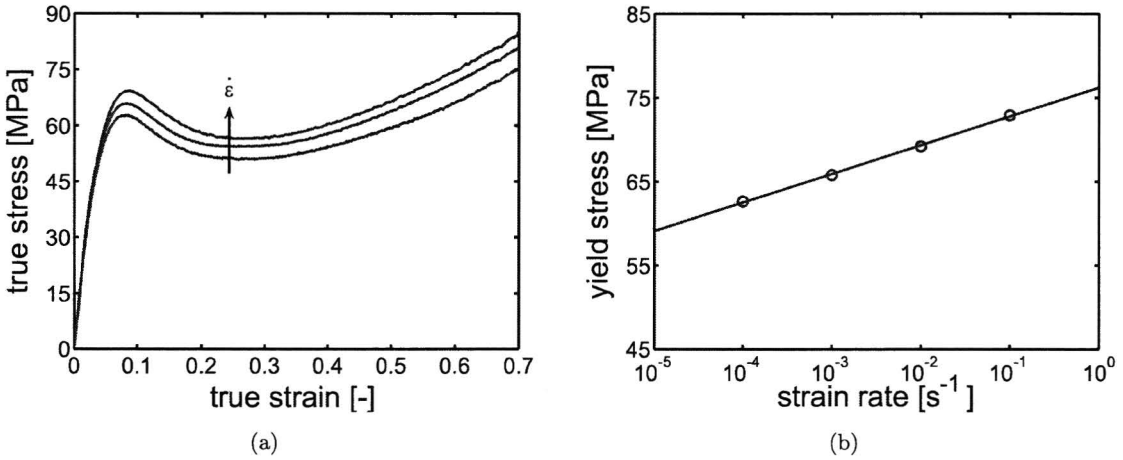

(a) (b)

Figure 2.2: *The influence of the strain rate on a compression curve (a) and the relation between yield stress and the strain rate for polycarbonate (b). Figures adapted from Klompen et al. [1, 2]*

The yield stress shows a linear dependency to the logarithm of the strain rate. The linear relation is two-directional. A prescribed strain rate gives a specific yield stress and the other way around an applied constant stress gives a constant characteristic strain rate at which the material will deform. The characteristic strain rate offers the possibility to predict the amount of accumulated plastic deformation in time for a prescribed stress. The flow after the yield point is not completely unrestricted, since during the flow the molecules orient, and at a certain point, increase the stress again as a function of the strain. In this study solely the deformation behaviour up to the strain softening is regarded.

Ageing kinetics

The second time-depending process that has to be regarded, relates to the ageing kinetics of the material. It is well documented in literature that polymers for mechanically unloaded conditions can show a decreasing molecular mobility termed physical ageing [10]. The influence of ageing on the material deformation behaviour is an increase of yield stress inducing a larger lifetime [1] and also the risk of brittle failure [1, 11]. The influence of the physical ageing on the deformation behaviour is shown in figure 2.1(b). Hence, in figure 2.3(a) the difference in yield stress induced by different processing histories is represented.

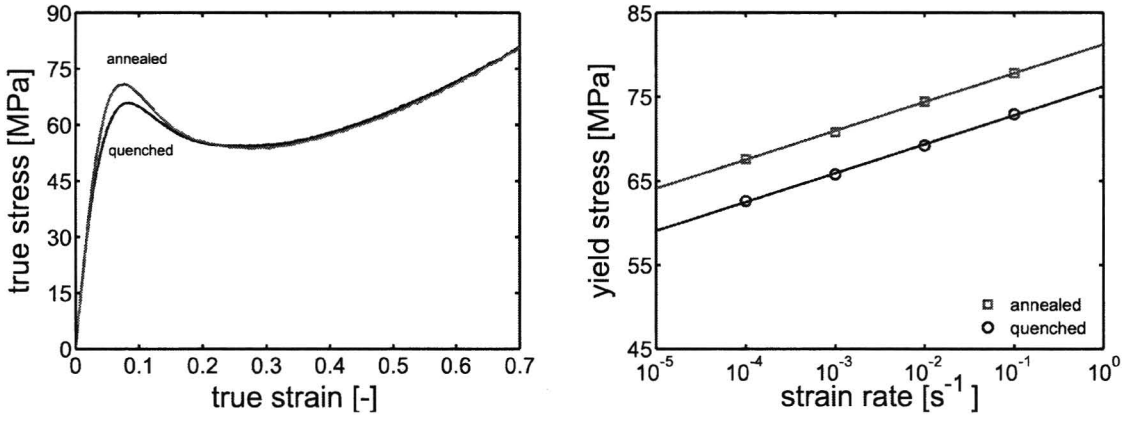

(a) (b)

Figure 2.3: *The influence of the initial age on the yield stress in a compression test (a) and on the relation between the yield stress and the strain rate (b) of polycarbonate. Figures adapted from Klompen et al. [1]*

The difference in yield stress as a result of different initial ages shifts the relation between the logarithm of the strain rate and the yield stress to lower strain rates for aged material, as shown in figure 2.3(b). As can be seen in the example, ageing is an important aspect in the lifetime prediction, since it has a profound influence on the rate of plastic deformation under given stress and temperature.

2.2 Intrinsic deformation of glassy polymers: modelling approach

A model describing the deformation behaviour of polycarbonate, has to take into account the deformation and ageing kinetics as witnessed in the experiments of Klompen et al. [1, 2]. In the approach the rate dependency was accurately captured by an Eyring flow rule. The softening and ageing of the material were described as a function of the accumulated plastic strain. In the full 3D-constitutive representation of the model the softening, the hardening and the pressure dependence are taken into account. The constitutive model is an elasto-viscoplastic model and is fully regarded in this chapter.

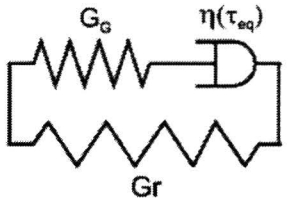

Figure 2.4: *General representation of the 3D constitutive model approach used by Klompen et al. [1, 2]*

The constitutive model

The 3D constitutive model makes use of a total Cauchy stress tensor that is decomposed to a driving stress ($\boldsymbol{\sigma}_s$) and a hardening stress ($\boldsymbol{\sigma}_r$) based on the approach of Haward and Thackray [12].

$$\boldsymbol{\sigma} = \boldsymbol{\sigma}_s + \boldsymbol{\sigma}_r \tag{2.1}$$

The hardening stress is described by a simple neo-Hookean relation

$$\boldsymbol{\sigma}_r = G_r \tilde{\boldsymbol{B}}^d \tag{2.2}$$

where G_r is the hardening modulus and $\tilde{\boldsymbol{B}}^d$ is the isochoric left Cauchy Green deformation tensor. The driving stress is decomposed into a deviatoric stress ($\boldsymbol{\sigma}_s^d$) and a hydrostatic stress ($\boldsymbol{\sigma}_s^h$) contribution.

$$\boldsymbol{\sigma}_s = \boldsymbol{\sigma}_s^h + \boldsymbol{\sigma}_s^d = K\left(J-1\right)\boldsymbol{I} + G\tilde{\boldsymbol{B}}_e^d \tag{2.3}$$

where G is the shear modulus, $\tilde{\boldsymbol{B}}_e^d$ the deviatoric part of the isochoric elastic left Cauchy-Green tensor, K the bulk modulus, J the volume change factor, and I the unity tensor. The superscripts d and h denote the *deviatoric* and *hydrostatic* contributions. The bulk modulus and the shear modulus are functions of the Young's modulus (E) and the poisson ratio (ν).

$$K = \frac{E}{3\left(1-2\nu\right)} \tag{2.4}$$

$$G = \frac{E}{2\left(1+\nu\right)} \tag{2.5}$$

The elastic volume change is captured by $\dot{J}$ in relation with the volume change factor J and the deformation tensor $\boldsymbol{D}$.

$$\dot{J} = Jtr\left(\boldsymbol{D}\right) \tag{2.6}$$

The Jaumann rate $\overset{\circ}{\tilde{\boldsymbol{B}}}_e$ is determined by the isochoric elastic left Cauchy Green deformation tensor $\tilde{\boldsymbol{B}}_e$, the plastic deformation rate tensor $\boldsymbol{D}_p$ and the deviatoric part of the driving stress tensor $\boldsymbol{D}^d$. The subscripts e and p denote the elastic and plastic contributions.

$$\overset{\circ}{\tilde{\boldsymbol{B}}}_e = \left(\boldsymbol{D}^d - \boldsymbol{D}_p\right) \cdot \tilde{\boldsymbol{B}}_e + \tilde{\boldsymbol{B}}_e \cdot \left(\boldsymbol{D}^d - \boldsymbol{D}_p\right) \tag{2.7}$$

The plastic deformation tensor $\boldsymbol{D}_p$ and the driving stress $\boldsymbol{\sigma}_s^d$ are related by a non-Newtonian flow rule. The viscosity is derived from an Eyring relation.

$$\boldsymbol{D}_p = \frac{\boldsymbol{\sigma}_s^d}{2\eta\left(T, p, \bar{\tau}, S\right)} \tag{2.8}$$

The model uses an equivalent stress.

$$\bar{\tau} = \sqrt{\frac{1}{2} tr\left(\boldsymbol{\sigma}_s^d \cdot \boldsymbol{\sigma}_s^d\right)} \tag{2.9}$$

The equivalent plastic strain rate is described by

$$\dot{\bar{\gamma}}_p = \sqrt{2 \cdot tr\left(\boldsymbol{D}_p \cdot \boldsymbol{D}_p\right)} \tag{2.10}$$

The viscosity depends on the equivalent stress ($\bar{\tau}$), pressure dependence (μ), absolute temperature (T) and the intrinsic state (S).

The nonlinearity of the model is governed by a single stress-activated viscosity defined in equation 2.11. The definition of the viscosity is of the same form as an Eyring viscosity, but next to a stress dependent shift factor (I), the contributions of hydrostatic pressure (II) and material state (III) are taken into account. The temperature dependency of the viscosity is governed in the definition of the initial viscosity and the characteristic stress.

$$\eta\left(T, p, \bar{\tau}, S\right) = \eta_{0,r}\left(T\right) \cdot \underbrace{\frac{\left(\bar{\tau}/\tau_0\right)}{\sinh\left(\bar{\tau}/\tau_0\right)}}_{I} \underbrace{\exp\left(\frac{\mu p}{\tau_0}\right)}_{II} \underbrace{\exp\left(S\right)}_{III} \tag{2.11}$$

with μ the pressure dependency, τ_0 the characteristic stress defined in equation 2.13 and T is the absolute temperature.

$$\eta_{0,r}\left(T\right) = A_{0,r}\tau_0 \exp\left(\frac{\Delta U}{R}\left(\frac{1}{T} - \frac{1}{T_{ref}}\right)\right) \tag{2.12}$$

In equation 2.12 the initial viscosity ($\eta_{0,r}$) is defined by the Arrhenius equation, where T_{ref} is the absolute reference temperature at which the parameters in table 2.2 are determined, $A_{0,r}$ is a constant concerning the jump-frequency at the reference temperature, R is the gas constant and ΔU is the activation energy. The characteristic stress (τ_0) is given by

$$\tau_0 = \frac{kT}{V^*} \tag{2.13}$$

where k is the Boltzmann constant and V^* is the activation volume.

The 3D constitutive model is used for isothermal simulations and uses a single set of parameters to describe the deformation behaviour for all grades of polycarbonate, listed in table 2.2 [1, 2].

E	900	$[MPa]$	τ_0	0.7	$[MPa]$
ν	0.4		S_a	-	
G_r	26	$[MPa]$	t_a	-	$[s]$
ΔU	295	$[kJ/mol/K]$	μ	0.08	
ΔU_a	205	$[kJ/mol/K]$	r_0	0.965	
V^*	5.78	$[nm^3]$	r_1	50	
V_a^*	2.21	$[nm^3]$	r_2	-5	
$\eta_{0,r}$	$2.1 \cdot 10^{11}$	$[MPa\ s]$	c_0	-4.41	
$A_{0,r}$	$3.0 \cdot 10^{11}$	$[s]$	c_1	3.3	

Table 2.1: *Model parameters for polycarbonate at a reference temperature of* $23°C$

The process of deformation is influenced strongly by a constant competition between the ageing and the rejuvenation of the material [2]. In the model the competition is captured by the parameter S. The parameter S consists of a contribution of the evolution of the material state (S_a) and the rejuvenation (R_γ) of the material defined in equation 2.15. Figure 2.5(b) represents the influence of the ageing and rejuvenation on the yield stress as function of the strain rate.

$$S\left(t, \bar{\gamma}_p\right) = S_a\left(t\right) \cdot R_\gamma\left(\bar{\gamma}_p\right) \tag{2.14}$$

$$R_\gamma\left(\bar{\gamma}_p\right) = \frac{\left(1 + \left(r_0 \cdot \exp\left(\bar{\gamma}_p\right)\right)^{r1}\right)^{\frac{r_2-1}{r_1}}}{\left(1 + r_0^{r1}\right)^{\frac{r_2-1}{r_1}}} \tag{2.15}$$

where r_0, r_1 and r_2 are model constants used to fit the function on experimental data [2]. The value of the softening (R_γ) is constant until a specific value for the accumulated plastic strain ($\bar{\gamma}$), after which R_γ decreases with increasing plastic strain.

The yield stress increases under influence of ageing and can be described as a function of the effective time, as was shown by Klompen et al. [2].

$$\sigma_y\left(t\right) = \sigma_{y,0} + c \cdot \log\left(\frac{t_{eff} + t_a}{t_0}\right) \tag{2.16}$$

where $\sigma_{y,0}$ is 23.4 MPa and c is 3.82 MPa for a strain-rate of $10^{-3}s^{-1}$ for polycarbonate concerning true stress. The effective time t_{eff} is defined in equation 2.18, t_0 is 1 s and t_a is the duration of the ineffective time before the ageing of the material sets in and follows a master curve as shown in figure 2.6(a).

$$t_a = \exp\left(\frac{S_a\left(0\right) - c_0}{c_1}\right) \tag{2.17}$$

where $S_a(0)$ is the initial value of the state parameter defined in equation 2.22 indicating the processing history of the material used.

The influence of temperature and stress are captured in the definition of the effective time (t_{eff}). In analogy with the stress-dependent shift function defined by Leaderman [13] and as used by Klompen et al. [2] for the viscosity, acceleration factors were defined by Klompen et al. [2] for the influence of

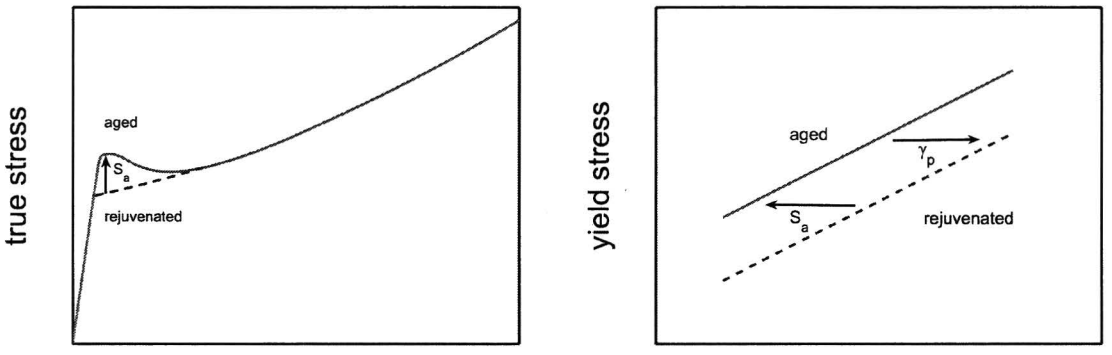

Figure 2.5: *Schematic representations of the state parameter S_a (a) and the competition between the influences of ageing and rejuvenation on the yield stress as a function of the logarithm of the strain rate (b). Figures are adapted from Klompen et al. [2]*

the temperature and stress on the effective time. The effective time is used to accelerate the evolution of the state parameter under influence of temperature and stress.

$$t_{eff}\left(T,\bar{\tau},t\right) = \int_0^t \frac{d\xi}{a_T\left(T\left(\xi\right)\right)\cdot a_\sigma\left(\bar{\tau}\left(\xi\right)\right)} \tag{2.18}$$

$$a_T\left(T\right) = \exp\left(\frac{\Delta U_a}{RT}\left(\frac{1}{T}-\frac{1}{T_{ref}}\right)\right) \tag{2.19}$$

$$a_\sigma\left(\bar{\tau}\right) = \frac{\left(\bar{\tau}/\tau_a\right)}{\sinh\left(\bar{\tau}/\tau_a\right)} \tag{2.20}$$

$$\tau_a = \frac{kT}{V_a^*} \tag{2.21}$$

where $\bar{\tau}$ is the equivalent stress, τ_a is the characteristic stress for ageing and V_a^* is the ageing activation volume.

The parameter S_a is used as an unique parameter in the model, describing the increase of the yield stress as a result of ageing of the material, as shown in figure 2.5(a). The initial value of the parameter S_a is obtained by fitting the yield stress from a tensile test simulation on the yield stress obtained experimentally by solely adjusting the S_a-value. The ageing of the material, captured by the state parameter, evolves as a function of time as is described by equation 2.22.

$$S_a\left(t\right) = c_0 + c_1\cdot\log\left(\frac{t_{eff}+t_a}{t_0}\right) \tag{2.22}$$

where c_0 and c_1 are constants listed in table 2.2.

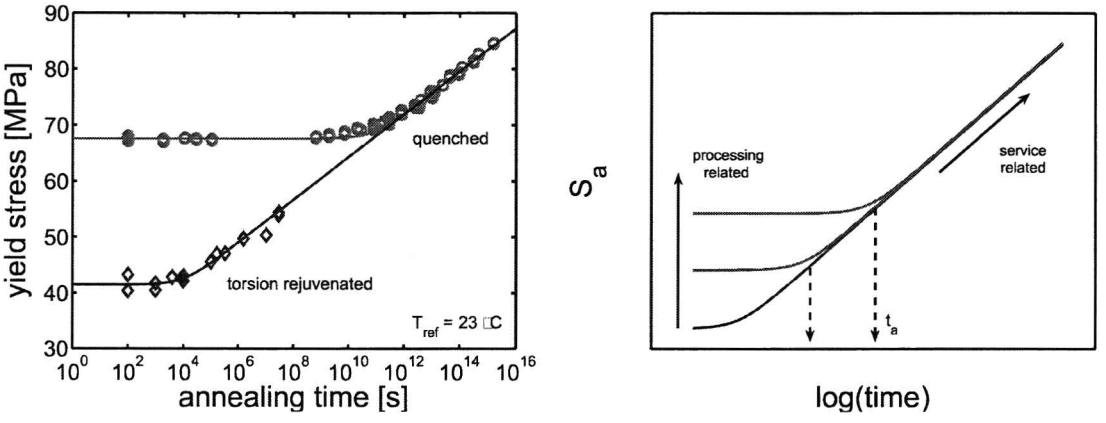

(a) (b)

Figure 2.6: *The quenched and torsion rejuvenated polycarbonate samples follow the same master curve for the evolution of the yield stress in time (a). Schematic representation of the influence of different processing histories on the state parameter evolution (b). Figures are adapted from Klompen et al. [1, 2]*

Application to polycarbonate

As is shown in figure 2.7(a) the 3D constitutive model can accurately predict the deformation behaviour of polycarbonate. The pre-yield behaviour is described linear elastic instead of non-linear viscoelastic as can be seen in the simulation of a compression test in figure 2.7(a). The elastic description is assumed not to influence the predictions for large deformations [9]. As shown in figure 2.7(a) the rate-dependency is accurate described by the model as well as the influence of the initial age as is shown in figure 2.7(b).

As was shown by Klompen et al. [1], the postulated 3D constitutive model can accurately predict the accumulation of plastic strain of the material under static loadings. Hence, the yield stress is obtained from tensile tests at varying strain rates, as is shown in figure 2.8(a).

The softening as function of the accumulated plastic strain offers an indication of the moment of failure of the material and allows the prediction of the fatigue lifetime. The influence of different initial age as well as the evolution of the yield stress is accurately predicted as shown for material of two different initial ages in figure 2.8(b).

2.3 Fatigue failure: status quo

Three parameters are taken into account as influence on the amount of accumulation of plastic strain and as a consequence the lifetime of the material. These three parameters are stress, temperature and processing history. The same list of parameters that influence the fatigue life can be made from literature, when reported experimental results are reviewed.

Fatigue failure of polymers is an active field of research. Many experimental results have been published and relations have been found to predict material behavior under cyclic loading conditions. A

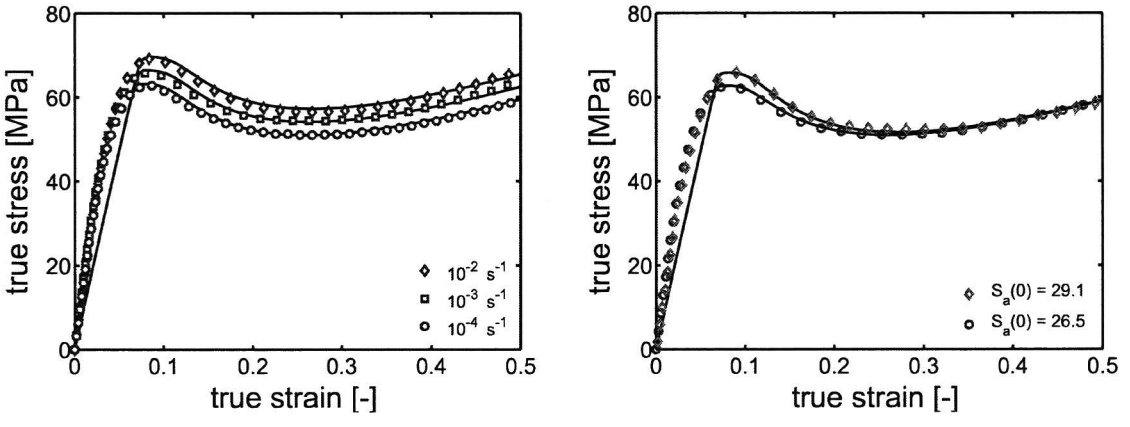

(a) (b)

Figure 2.7: *The experimental data and simulations of compression tests at different strain rates (a) and for different initial ages (b) for polycarbonate. Figures are adapted from Klompen et al. [1, 2]*

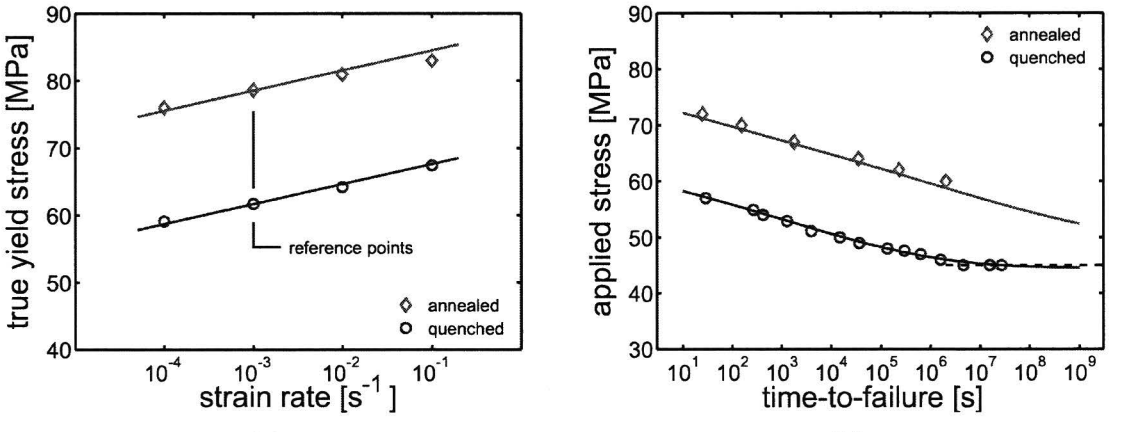

(a) (b)

Figure 2.8: *Measurements of the yield stress at different strain rates (a). Predictions of the lifetime of polycarbonate of different initial ages (b). Figures are adapted from Klompen et al. [1, 2]*

variety of experimental methods is used in literature, differing in shape of the stress loading (sine, block) as well as the way the stress loading is altered e.g. changing the ratio between the maximum and minimum of the stress signal, different amplitudes around a constant mean stress or different in tensile, compression or tensile-compression tests. An extensive review on this subject is given by Lesser [14]. A short overview on the proceedings and conclusions in literature is given to indicate the premises of this thesis.

The fatigue failure measurements in the work of Lesser [15, 16] are based on nylon and polyacetal. In

this work a sine shaped stress signal in tensile direction is used as shown in figure 3.1(a). Fatigue life measurements are typically plotted in cycles to failure as function of the applied stress, as is commonly accepted in metal studies and known as Wöhler curves. A distinction is made in the results of Lesser, shown in figure 2.9, between *high cycle* and *low cycle fatigue*. Low cycle fatigue is dominated by overcritical (hysteretic) heating of the polymer, *thermally dominated region*, leading to a drop in the viscosity and inducing irreversible viscous flow. High cycle fatigue, *mechanically dominated region*, called the *true fatigue* response by Lesser, is explained by accumulated material damage or crack growth. Lesser noticed in between the low and high cycle fatigue a large plateau, where the mode of failure changed from ductile failure to brittle rupture. In chapter 4 the results of Lesser are discussed in more detail.

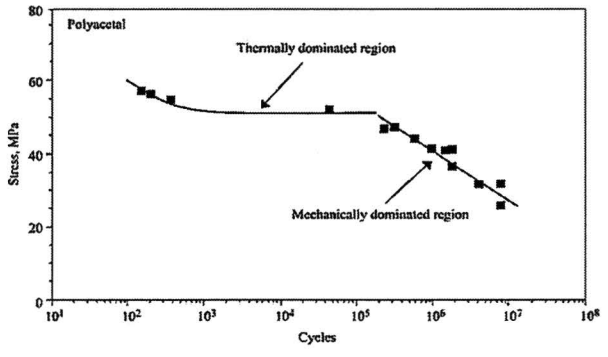

(a)

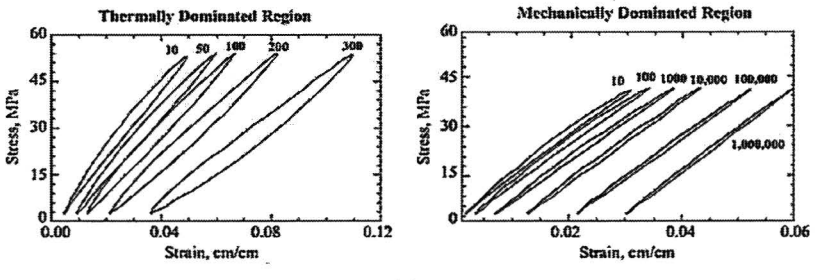

(b)

Figure 2.9: *Fatigue life measurements on polyacetal (a) and hysteresis loops for two specific stresses (b). Figures are adapted from Lesser et al. [15, 16].*

More extensive work on the variables influencing the fatigue life measurements, is performed by Benham and Crawford [17, 18]. Benham and Crawford performed measurements on a serie of polymers and reported on a transition stress equal to the transition stress observed by Lesser. At this specific stress Benham and Crawford notice a balance to exist between the increase of the temperature by hysteretic heating and the heat loss through convection as shown in figure 2.10(a). The study focusses further on the frequency, the shape, the mean value and the amplitude of the stress. The temperature was studied during the fatigue loadings as shown in figure 2.10(b). All variables are discussed in the results in chapter 4.

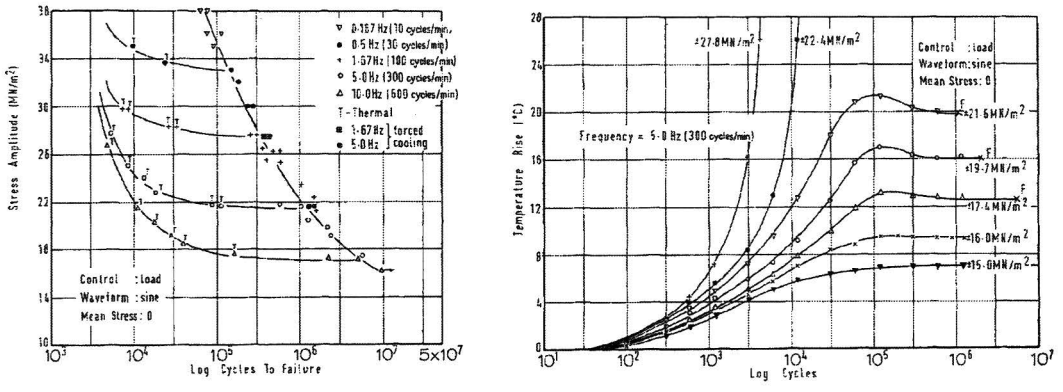

(a) (b)

Figure 2.10: *Fatigue and thermal failure curves (a) and the specimen temperature rise (b) in cyclic tension-compression tests on polycarbonate. Figures are adapted from Crawford and Benham [17].*

The change of material properties through ageing under influence of stress and temperature, is widely reported in literature [1, 2, 19–26]. A good overview on ageing is given by Hutchinson [10]. Ageing was reported by changes in for example density, relaxation modulus and a decrease of the loss tangent. Yee et al.[21] performed measurements on polycarbonate and reported that physical ageing and ageing under fatigue loading show many similarities. Irrespective of the great resemblance in ageing, Yee considered them different since the physical ageing showed a decrease of average hole size and fatigue ageing showed an increase of the average hole size in the material.

It can be concluded from literature that stress, temperature and processing history have all influence on the fatigue life of polycarbonate. These three parameters are individually discussed in the experimental results.

2.4 Scope of thesis

It was demonstrated in this chapter that a full 3D constitutive model is available to accurately describe the deformation behaviour of polymers under short- and long-term constant loadings or strain rates. Klompen et al. [1, 2] pointed out that three parameters influenced the failure behaviour of polycarbonate: stress, temperature and processing history. All three are introduced as parameters on the viscosity. The influence of the stress and temperature are introduced as influences on the time of the evolution of the yield stress. The scope of this thesis is to study the possibilities to use the constitutive model to describe the deformation behaviour of polycarbonate under short- and long-term cyclic loadings. The approach of Klompen et al. [1, 2] is used to predict the fatigue life.

Chapter 3

Materials and methods

In this chapter the materials and experimental techniques used, are discussed. In this study polycarbonate is used as material for the experiments and simulations. Tensile tests are used to determine the thermal history of a material and to follow the evolution of the yields stress during the experiments. The temperature is measured by infrared temperature sensing techniques.

3.1 Materials

The materials used, are commercial grades of polycarbonate. Measurements were performed on Lexan 101R, 141R and 161R supplied as granules by GE Plastics and Makrolon supplied as extruded plate by Bayer. The granules are dried for 24 hours at 80°C in an air circulated oven prior to processing to prevent degradation. The samples used to obtain experimental data are produced according to the ASTM D638 – 91 and ISO 527 – 1B/A norms. Makrolon samples obtained from extruded plates are machined into the ASTM D638 – 91 norm. The samples of Lexan 101R, 161R and 141R are obtained from injection moulding and the norms used are listed in table 3.1. The molecular weight distributions are reported by Klompen [1, 2] and also listed in table 3.1.

To study the effects on the fatigue lifetime of the material, samples with different thermal histories are created. To achieve this, Lexan 141R is injection moulded at two different mould temperatures of 30°C and 130°C. The Lexan 101R and 161R samples are all produced with a mould temperature of 30°C and subsequently a selection is annealed at 120°C in an air circulated oven for over 72 hours. The

Grade	Thickness	Mold temperature	Annealing	S_a [-]	M_n [kg/mol]	M_w [kg/mol]
Lexan 101R	1 mm	$30°C$	-	27.3	12.7	28.9
Lexan 101R	1 mm	$30°C$	-	29.7	12.7	28.9
Lexan 101R	1 mm	$30°C$	72h $120°C$	43.6	12.7	28.9
Lexan 161R	1 mm	$30°C$	-	27.5	11.6	27.9
Lexan 161R	1 mm	$30°C$	72h $120°C$	42.2	11.6	27.9
Lexan 141R	3 mm	$30°C$	-	29.5	9.2	25.8
Lexan 141R	3 mm	$130°C$	-	33.8	9.2	25.8
Makrolon	3 mm	-	-	27.5	8.2	18.7

Table 3.1: *Overview of the properties of the polycarbonate grades used in this study. The molecular weights are adapted from Klompen et al. [1, 2].*

Lexan 101R samples keep the initial dimensions after the annealing treatment in contrast to Lexan 161R samples that reduce in dimensions by less than 1%.

3.2 Experimental techniques

Tensile testing

The tensile tests are performed on servo-hydraulic MTS Elastomer Testing Systems 810 and 831.10. The specimens are tested at constant linear strain rates of 10^{-2}, 10^{-3} and 10^{-4} s^{-1} at room temperature. Samples are acclimatised in the temperature chamber for at least 10 minutes.

Creep and cyclic fatigue testing

The creep and fatigue tests are performed on servo-hydraulic MTS Elastomer Testing Systems 810 and 831.10. To exclude the effect of temperature changes, an air-temperature controlled chamber at a constant temperature of 23°C is used. Creep tests are performed on Lexan 161R and fatigue tests are performed on Lexan 101R, 141R, 161R and Makrolon. The moment of failure of the polycarbonate samples is defined as the moment in time, where necking or brittle failure is observed.

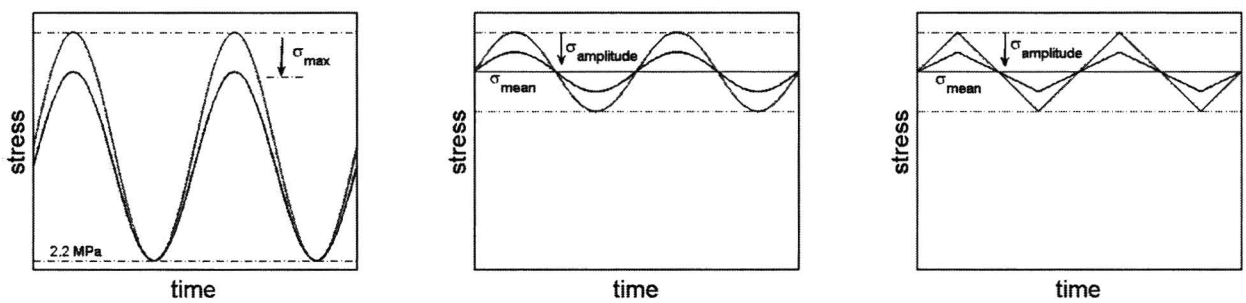

Figure 3.1: *Three types of dynamic stress signals are used in this study: a dynamic stress signal with a variable large, sine shaped stress amplitude (a), a fixed small amplitude (b) and a sawtooth shaped small amplitude (c).*

Three types of dynamic loading signals are used in the experiments. The sine shaped signal in figure 3.1(a) is adapted from the work of Lesser [15, 16] and will further be referred to as *large amplitude stress signal.* The maximum stress is variable, but the minimum stress is fixed at 2.2 MPa. A second dynamic stress signal shown in figure 3.1(b), is used to validate predictions for small amplitudes and is in this study referred to as *small amplitude stress signal.* The mean stress is variable and the amplitude is taken constant at 5 MPa. Equal to figure 3.1(b) a sawtooth shaped stress signal, shown in figure 3.1(c), is used to investigate the ability of the model to predict different dynamic stress shapes. The stress signals are prescribed in the experiments in engineering stress. To study the influence of the frequency, Makrolon samples are subjected to the frequencies of 2 and 10 Hz.

Isothermal dynamic measurements

An in-house designed and constructed set-up is built to approach isothermal conditions. The set-up is designed to be used in combination with the dynamical testing systems. The set-up consists of cylindrical, plexiglas column with a diameter of 60 mm and is filled with 900 ml water. The design allows the addition of an external waterpump to control waterflow and temperature. The column allows measurements on ASTM D638 – 91 samples, but was optimised and used for ISO 527 – 1B/A samples. The pump used in fatigue life experiments has a maximum flow of 0.045m/s and pumps water from an open water container, without temperature control. Tap water is manually added to control the water temperature. The water pump is replaced in the fatigue ageing measurements by a $M12$ Lauda water container, with a $MS/2$ Lauda temperature controller and water pump. The temperature is controlled at 22°C. The water flow is kept constant at 0.045 m/s. The effect of the water in the column on the measurements was investigated. Measurements showed an influence of the water on the force registration with a maximum of approximately 0.5 N, which is negligible to the forces used in the experiments. The effect of the water in long term measurements on the properties of the polycarbonate, samples were placed in water for more than 72 hours at room temperature and afterwards the yield stress was measured. No influence of the water on the yield stress compared to the yield stress of dry samples, was observed.

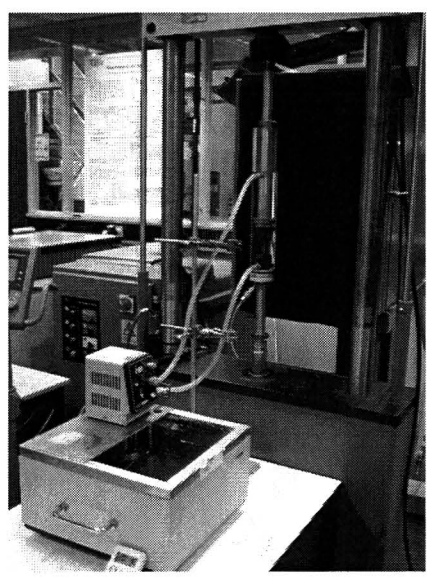

Figure 3.2: *The in-house designed set-up used to approach isothermal conditions.*

Thermography

The infrared measurements are performed with a ThermaCAM PM575 from FLIR Systems. The infrared temperature sensing technique uses the radiation of the sample to measure the temperature. The camera is calibrated on the intensity of the radiation of a black-body radiator. Since samples do not comply with a perfect black-body radiator, the camera has to be adjusted for the experimental set-up conditions.

Three factors influence the amount of radiation transmitted by a sample: the spectral absorptance (α), the spectral reflectance (ρ) and the spectral transmittance (τ). Kirchhoff's Law states the absorptance of the material to be equal to the emissivity (ε) on every temperature and wavelength. The relation between the three contributions is given by equation 3.1 where the emissivity is used instead of the absorptance.

$$\varepsilon + \rho + \tau = 1 \tag{3.1}$$

It is shown by Koenen [27] that the thermal intensity measured by the camera can be described as a function of a reference intensity from the black-body at a specific temperature and the three contributions as shown in equation 3.2.

$$I_m = \varepsilon I_b\left(T_m\right) + \rho I_b\left(T_s\right) + \tau I_b\left(T_s\right) \tag{3.2}$$

where I_m is the intensity of the material, I_b the intensity of the black-body, T_m the absolute temperature of the sample and T_s the absolute temperature of the surroundings.
Using equation 3.1 and 3.2 leads to a definition for the intensity of a black-body at a temperature equal to the sample as shown in equation 3.3.

$$I_b\left(T_m\right) = \frac{1}{\varepsilon} I_m + \left(1 - \frac{1}{\varepsilon}\right) I_b\left(T_s\right) \tag{3.3}$$

With the known relation between the intensity of the black-body and the temperature, from the calibration, a material temperature can be derived. A calibrated K-thermocouple was used to obtain a value for the emissivity for the polycarbonate samples. The temperature measured by the camera was compared to the temperature of the thermocouple and the value of the emissivity was adapted until the temperatures were equal for all temperatures in the range of interest. The emissivity of the material is known to change as function of the temperature. At higher temperatures the emissivity of the material is lower. Within the measured temperature range the emissivity is assumed not to change significantly and is set on a constant value of 0.95. This value was also determined for polycarbonate at room temperature by Koenen [27].

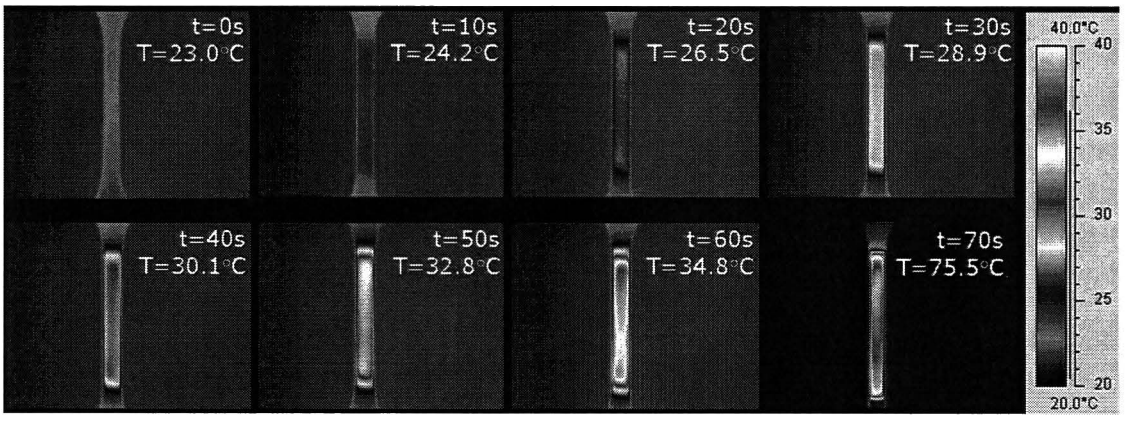

Figure 3.3: *Example of infrared measurements on Lexan 141R.*

The ThermaCAM measures within the spectral of 7.5 and 13μm, with an atmospheric filter cutting at 7.5μm. Measurements are performed at a distance of 0.6 m to minimise atmospheric radiation. The humidity is set constant at 33% and measurements are performed at room temperature. The infrared temperature measurements have a stated accuracy of 0.1°C.

The infrared temperature sensing technique is chosen since the technique has the advantage of no interference with the sample during measurements. The technique provides a rapid measurement of the surface temperature. An alternate method would be the use of a thermocouple. Since the thermocouple is cooled by the surroundings, the measurements are slower and result in a lower temperature increase measurement. When samples are relatively thin, the infrared measurements give a better representation of the bulk temperature of the sample. Thicker samples have a temperature gradient over the thickness of the sample. Rabin and Rittel [28] showed that for the 3 mm thick ASTM-norm samples, the difference between core temperature and wall temperature is less than 5%. The difference between core and wall temperature was determined to be less than 1% for the 1 mm thick ISO-norm samples. During fatigue loadings heat is generated within the sample and the percentages can increase. On the other hand, as shown in appendix A, both samples have a Biot number lower than 0.1, suggesting an uniform temperature distribution between core and surface. The Biot number is a nondimensional parameter that gives a ratio between the convection and the conduction as shown in equation C.4.

Chapter 4

Experimental results

In this chapter the experimental results for fatigue failure are compared to the results and conclusions from literature [14–16, 20, 21]. Also the role of processing history, stress and temperature on the time to failure are discussed.

General observations

Corresponding to the experiments performed on polyacetal by Lesser [14–16] shown in figure 2.9, fatigue measurements on polycarbonate are performed with the stress signal given in figure 3.1(a). The results in figure 4.1(a) show a clear similarity to the results of Lesser. A first characteristic observation is the distinct plateau at 57 MPa that indicates the transition between low and high cycle fatigue. The relation between the lifetime and the stress is determined by the material state as shown in figure 4.1(b). The curve for annealed samples with a S_a-value of 33.8 shifts to higher stresses compared to the quenched samples with a S_a of 29.5.

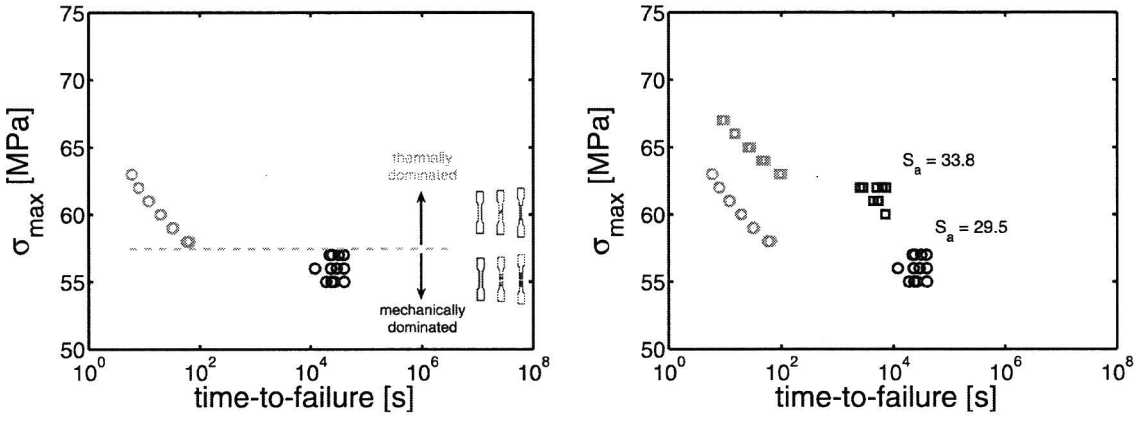

(a) (b)

Figure 4.1: *Fatigue life measurements on Lexan* $141R$ *with a* S_a *of* 29.5 *(a). Fatigue failure measurements for Lexan* $141R$ *for two different thermal histories (b).*

The samples show around the stress level of the plateau also a clear transition from ductile failure (necking, low cycle) to brittle rupture (high cycle). The indications of thermally and mechanically

dominated regions in figure 4.1(a), as proposed by Lesser in figure 2.9, are better understood when the results shown in figure 4.2 are taken into account which show the increasing temperature and the energy dissipation of the samples during fatigue.

In figure 4.2(a) and 4.2(b) the evolution of the hysteresis loops are shown for two distinct situations. Figure 4.2(a) shows the hysteresis loops for a maximum stress of 59 MPa, in the thermally dominated region. The loops for 59 MPa enclose large areas, indicating a constant and large energy dissipation during the fatigue loading. The energy dissipated leads to an increase of the temperature of the material and as a consequence shortens its fatigue life. In figure 4.2(b) the hysteresis loops are shown for the maximum stress of 56 MPa, from the mechanically dominated region. Compared to the hysteresis loops of 59 MPa the loops of 56 MPa show the opposite. The enclosed area within the loops is not constant or increasing, but decreases with increasing time. The decrease of enclosed area indicates a decrease of energy dissipation and will not lead to a continuous increase of the temperature of the material as expected for 59 MPa.

In figure 4.2(c) the dissipated energy is shown for all measurements presented in figure 4.1(a). The evolution of the hysteresis loops shown for 59 and 56 MPa can also be observed in figure 4.2(d). The energy dissipation for maximum stresses *above* 57 MPa show an almost constant energy dissipation, with a strong dissipation increase prior to failure induced by the softening of the material. The dissipated energy for samples of 57 MPa and lower show a continuous decrease. Remarkable is the change of slope for the dissipated energy at a time of approximately 100 seconds. A likely explanation is ageing of the material incorporating a decrease of the loss compliance and subsequently a decrease of the dissipated energy [20, 21, 25, 26]. The increase of age embrittles the polycarbonate and explains the transition in the type of failure from ductile to brittle rupture [11].

The temperature increase of the material is shown in figure 4.2(d). In this figure again the difference between the thermally and mechanically dominated regions is observed. The maximum stresses from the thermally dominated region *above* 57 MPa show a continuous increase of temperature until failure, indicated by x in the figure. On the other hand, the maximum stresses of the mechanically dominated region show a balance between the increase of the temperature and the heat lost to the surroundings. To be noticed is the decrease directly after the balance point in the temperature. If a stable balance was found between the heat generation and heat loss to the surroundings the temperature is expected to stay constant. The decrease of temperature is likely a consequence of the ageing of the material. The ageing increases the yield stress and as a consequence the energy dissipation will decrease.

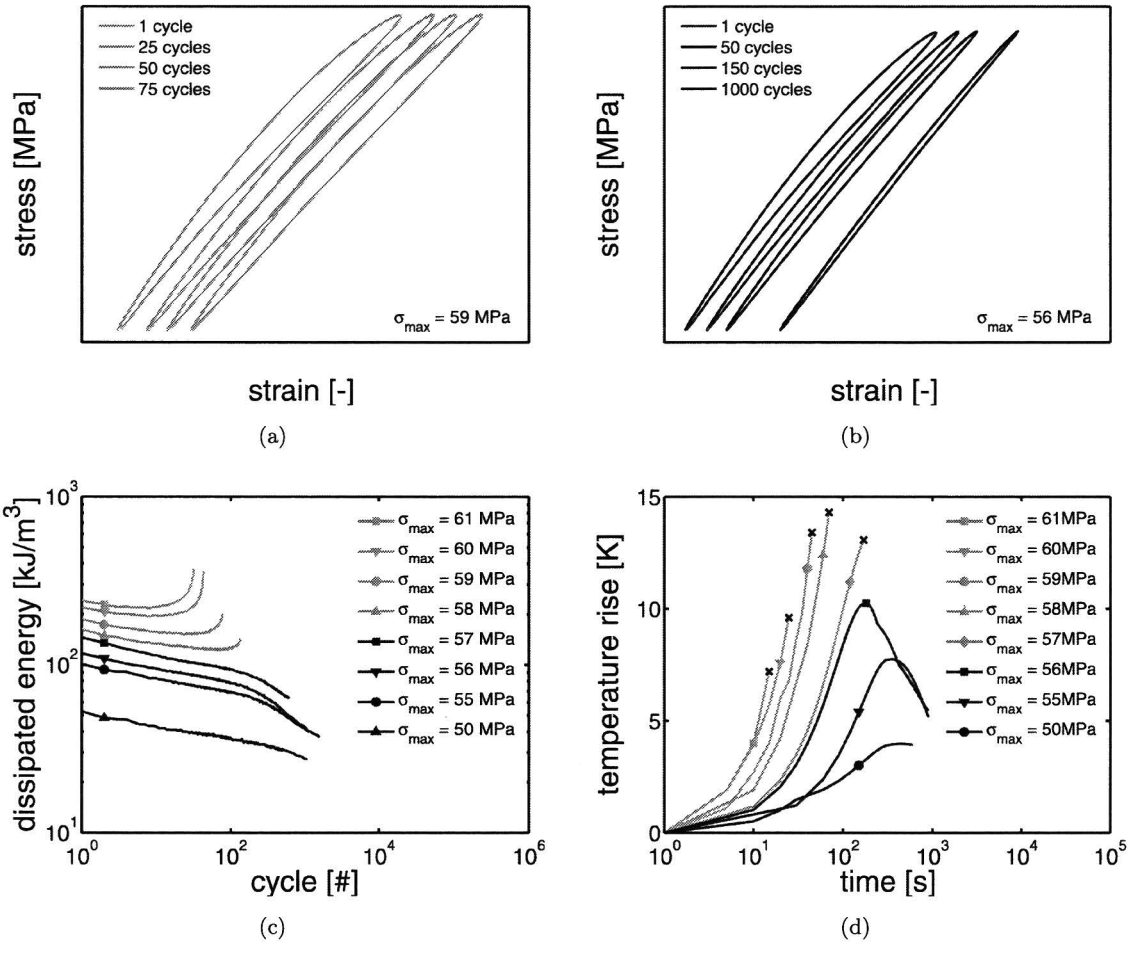

Figure 4.2: *Measurements are performed on Lexan* $141R$ *with a* S_a *of* 29.5. *Evolution of the hysteresis loops for a maximum stress of* 59 *MPa (a) and* 56 *MPa (b). Measured dissipated energy per cycle (c). Temperature measurements on the surface of the sample using infrared thermography (d).*

Fatigue failure: frequency

The influence of frequency is often said to be taken into account in experiments, but experimental evidence is seldom published. Crawford and Benham [17, 18] state that the frequency influences the lifetime of the samples, when the results are shown in a Wöhler curve. In figure 4.3(a) the results for two frequencies are shown and a clear shift in the results is observed. On the other hand in figure 4.3(b) where the same results are plotted as a function of time, no difference is found for the two frequencies.

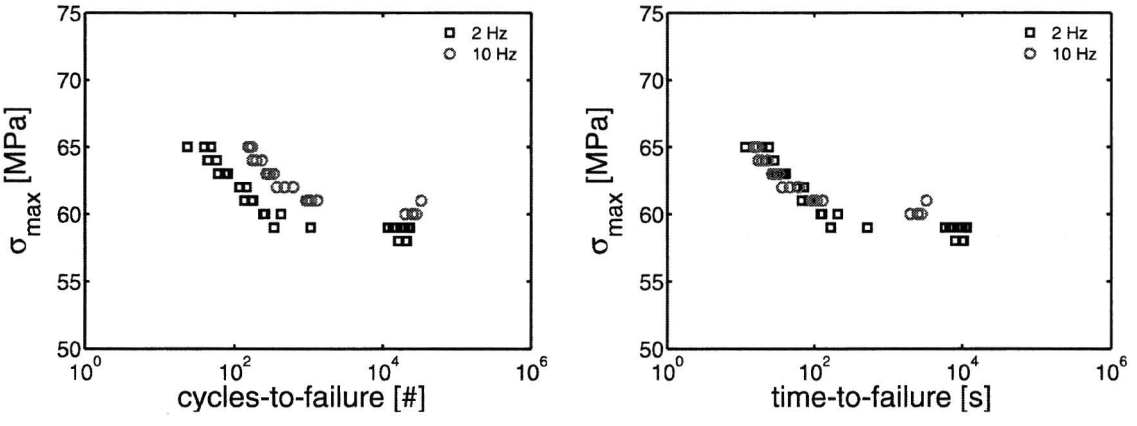

Figure 4.3: *Measurements are performed on Makrolon with a S_a of 27.5. Fatigue life measurements for two frequencies typically plotted against the cycles (a) and the time (b).*

The time of failure of a material is determined by the accumulation of plastic strain. Ignoring for a first moment the effects of heating of the sample, over a second of time the amount of accumulated plastic strain for 2 and 10 Hz predicted by the model is equal. Therefore, under isothermal conditions the results of 2 and 10 Hz should overlap. Since figure 4.3 shows the results for the thermally dominated region, the temperature increase of the material has also to be taken into account.

In literature [14, 29] the energy dissipation and the temperature increase are defined as a function of the frequency, the loss compliance and the stress amplitude.

$$\frac{dQ}{dt} = f\pi\sigma_d^2 D''(f,T,t) \tag{4.1}$$

$$\frac{dT}{dt} = \frac{dQ}{dt}\cdot\frac{1}{c_p\rho} \tag{4.2}$$

where Q is the dissipated energy, f the frequency, σ_d is the stress amplitude, D" the loss compliance, T the absolute temperature, c_p the heat capacity and ρ the material density.

If the loss compliance would have been constant, the temperature would increase with increasing frequency and lead to shorter a lifetime for higher frequencies. As can be seen in the results in figure 4.3(b) the results overlap. This suggests that with increasing frequency the dissipated energy equally decreases or regarding equation 5.12 the loss compliance. The amount of energy dissipated is influenced by more than one parameter and is therefore a complex subject. In this study the frequency is taken 2 Hz in all experiments and is not further investigated.

The polycarbonate has a low heat conduction and in relative thick samples a temperature gradient can exist between the core and the surface of the sample. By reduction of the minimum distance of conduction in the sample, the temperature gradient between the core and the surface of the sample is minimised. Hence, in the results in the next sections, ISO-norm samples with a thickness of 1 mm are used instead of the 3 mm thick ASTM-norm samples.

Fatigue failure: quenched material

In figure 4.4 the fatigue life measurements are shown for quenched Lexan 101R samples. In figure 4.4(a) a linear relation is found for low cycle fatigue. At a maximum stress of 55 MPa failure is no longer observed during the time of measurement. Considering the temperature increase measurements in figure 4.4(b), the observations are similar to the results earlier in figure 4.2(d). However, the results in figure 4.4(b) show a stronger increase and decrease of the temperature. The dissipated energy for 56 and 55 MPa in figure 4.4(c) decreases after 50 seconds, again suggesting almost instant ageing of the material. To visualise the ageing of the material the evolution of the yield stress is measured during fatigue, since the ageing influences the yield stress as shown by equation 2.16. Samples are fatigued for specific numbers of cycles and afterwards, the yield stress is determined by tensile testing at a strain rate of $10^{-3}s^{-1}$. The maximum stress is taken at 50 MPa to ensure that no failure occurs before 10^6 s. The yield stress increases as shown in figure 4.4(d), affirming the suggestion of ageing.

Fatigue failure: annealed material

The results for the annealed samples are shown in figure 4.5. It is striking that there is a linear relation between maximum stress and the logarithm of the time to failure in figure 4.5(a). The increase of temperature for the annealed samples in figure 4.5(b) is slower than observed for the quenched samples, but still reaches the same maximum value of 4°K before failure, as the quenched samples in figure 4.4(b). For a maximum stress of 72 MPa, a point of stabilisation of the temperature is observed, indicating a balance between the heat generation and loss of heat to the surroundings. In the results for Lexan 101R in figure 4.4(c) a change of slope was observed in the dissipated energy explained by the ageing of the material. In figure 4.5(c) the dissipated energy for annealed Lexan 101R shows a constant decrease for all stresses, but no change of slope is observed indicating ageing.

Fatigue failure: isothermal

The results for the quenched samples in figure 4.4(a) and annealed samples in figure 4.5(a) are shown again in figure 4.6 and compared to the results of the samples loaded in water during the fatigue loading. The samples were loaded in water to increase the loss of heat to the surroundings. The results for the quenched samples in figure 4.6(a) show a large increase of the lifetime compared to the samples

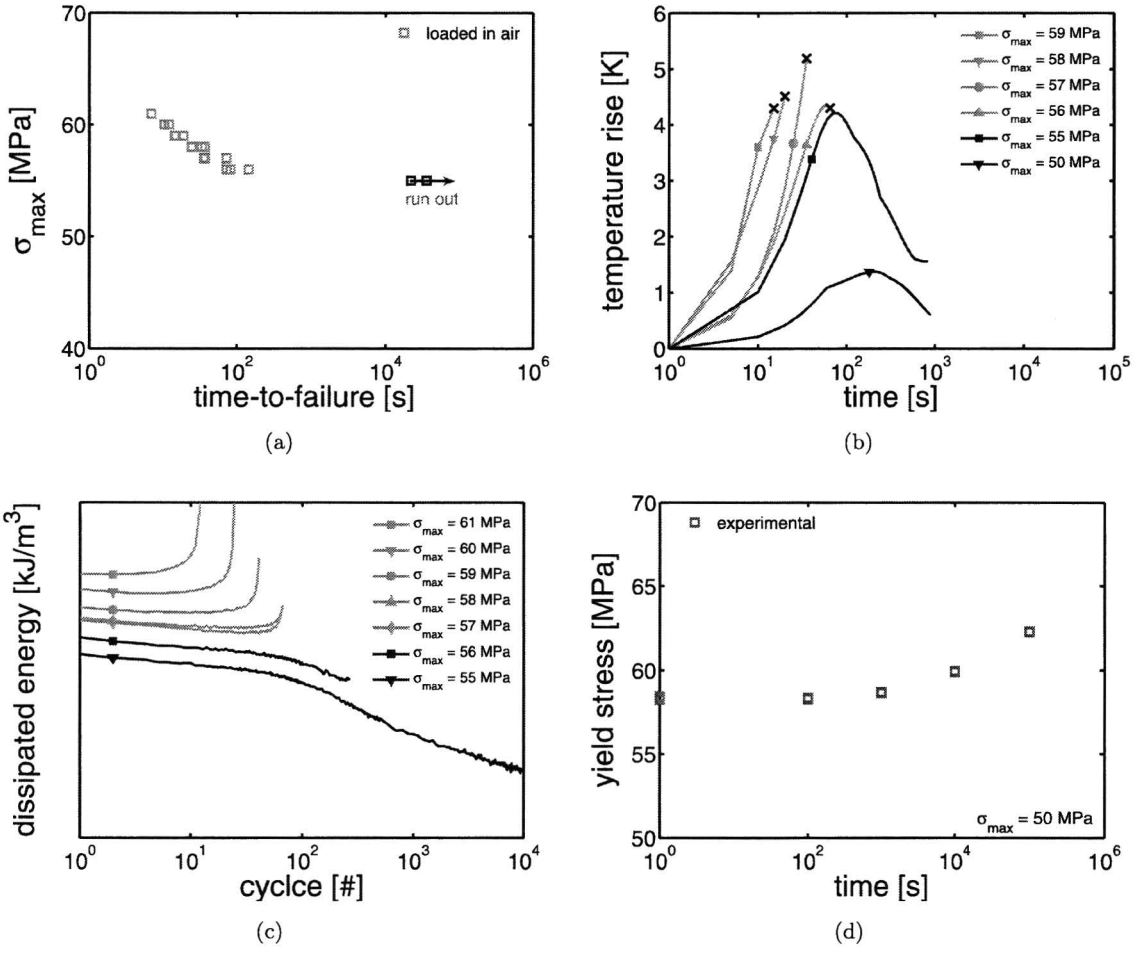

Figure 4.4: *Measurements are performed on quenched Lexan* $101R$ *with a* S_a *of* 27.3. *Fatigue lifetime (a) and infrared temperature measurements (b). Measured energy dissipation (c) and the increase of the yield stress under cyclic loading (d). Run out: no failure during the time of measurement.*

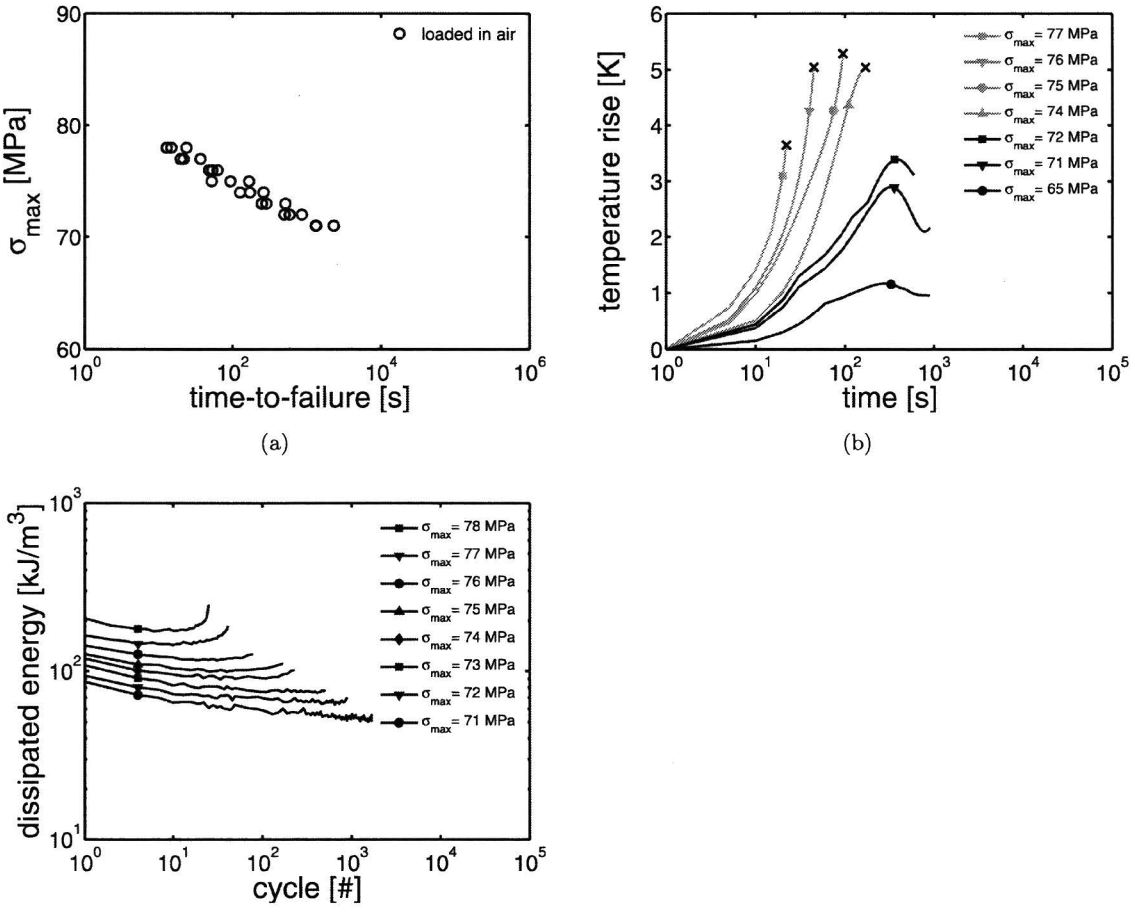

Figure 4.5: *Measurements are performed on annealed Lexan* $101R$ *with a* S_a *of* 43.6. *Fatigue lifetime (a) and infrared temperature measurements (b). Measured energy dissipation under cyclic loading (c).*

loaded in air. The results for the quenched samples loaded in water show an almost linear relation between the logarithm of the time to failure and the maximum stress applied. Regarding the annealed samples in figure 4.6(b) only a small difference between the measurements of samples loaded in air and in water is observed. However, the conclusion can not be drawn that the samples do not heat at all, since the samples loaded in air showed heating in figure 4.5(b) and the differences in time to failure compared to the samples loaded in water, are small. Apparently, small temperature increases do not always visibly affect the lifetime of the annealed material. Unfortunately the used water column makes it impossible to use infrared temperature sensing to measure the temperature increase of the samples loaded in water.

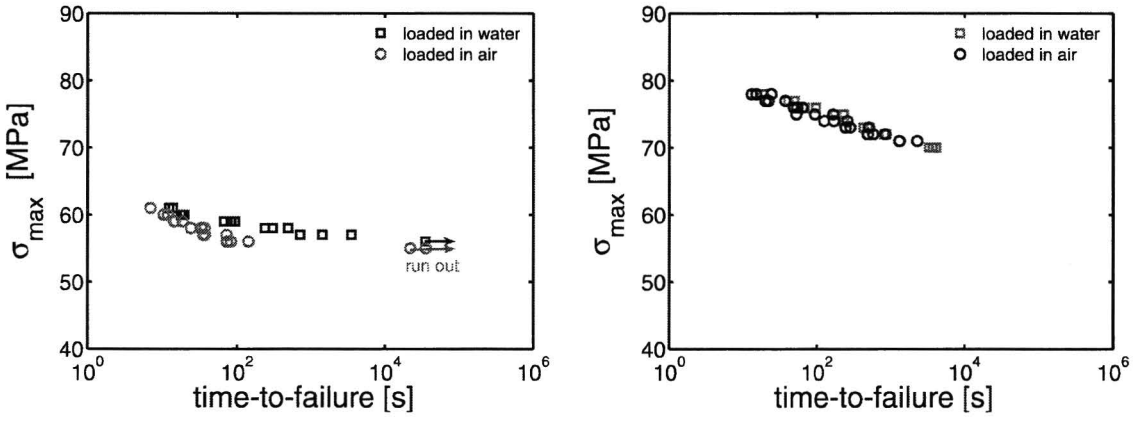

Figure 4.6: *Fatigue life measurements for quenched ($S_a = 27.3$)(a) and annealed ($S_a = 43.6$)(b) Lexan 101R loaded in air and water. Run out: no failure during the time of measurement.*

Summary experimental results

The experimental results have shown the influence of three factors on the fatigue life of polycarbonate: stress, temperature and processing history. The experiments showed clear plateau's in the measurements for polycarbonate with a low S_a-value. The characteristics of fatigue lifetime measurements described in literature are also observed in the experiments on polycarbonate. Thermally and mechanically dominated regions are present in the experimental results and a plateau in between the regions was noticed. The plateau is determined by the balance between heat generation in the sample and the heat loss to the surroundings. The transition in failure modes observed in the measurements is explained by ageing of the material. An influence of the frequency on the fatigue lifetime is not observed.

Chapter 5

Numerical results

5.1 Predictions on the fatigue lifetime

The 3D-constitutive model as formulated by Klompen et al. [1, 2] is used in this study with the FEM-package MARC for isothermal simulations to predict creep and fatigue lifetimes. The fatigue simulations with MARC directly proved expensive in memory and CPU-time. On the other hand the simulations of static loading conditions proved to go relatively fast. Simulations of static loading conditions can be performed fast due to computation techniques such as adaptive time-stepping. Adaptive time-stepping allows variable time-steps to be used in the simulations as long as convergence criteria are reached.

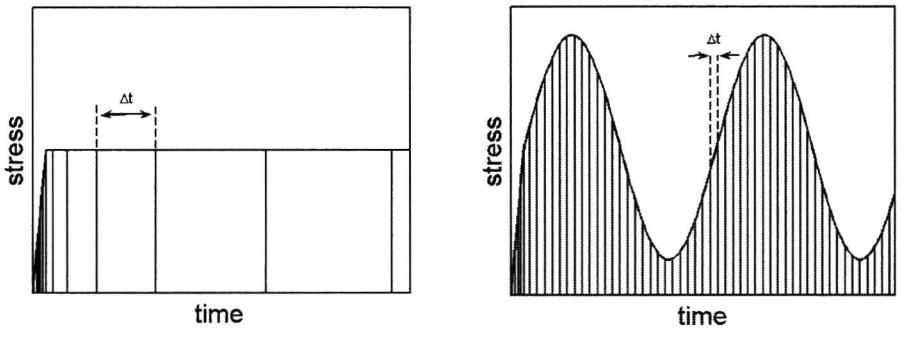

Figure 5.1: *Schematic representations of the time-steps taken in adaptive time-stepping for a static stress (a) and the constant, minimum time-steps for a cyclic stress (b).*

The adaptive time-stepping reduces computation time and makes fast creep simulations possible. In case of cyclic loadings or changes in temperature, the time of calculation increases rapidly in expense, since it is no longer possible to use techniques as adaptive time-stepping. Since at least 64 points are needed to describe e.g. a sine shaped stress signal, this gives a time step of $7.8125 \cdot 10^{-3}$ s at 2 Hz. Hence, fatigue simulations in MARC can only be performed until 10^3 seconds. All time-steps have to be predefined in the program as well as all cycles, since MARC offers no possibilities to repeat prescribed stress cycles. The large amount of data points that has to be stored, becomes a problem for the memory, when simulations become larger than 10^3 s. For high cycle fatigue simulations of 10^4

cycles and more, a solution has to be found. The increase of the computation time in MARC is shown in figure 5.2. As example a MARC simulation for a sawtooth shaped stress signal with two different amplitudes at a frequency of 1 Hz, is compared to a simulation of a static stress signal using adaptive time-stepping.

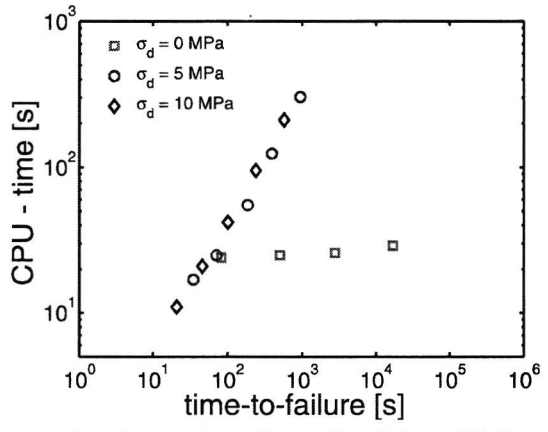

Figure 5.2: *Computation time against the predicted time of failure for simulations on polycarbonate in MARC with a 3D constitutive model. A sawtooth shaped stress signal at 1 Hz was prescribed to a 1-element model.*

The current implementation in MARC is used for isothermal fatigue simulations. The experimental results for annealed Lexan 101R shown in figure 4.6(b) are used to validate the isothermal simulations. These experimental results are used, since they showed no indications of influence of temperature or ageing on the time to failure. The simulations are performed in MARC at a reference temperature of 22°C, while the fatigue life experiments were performed with samples loaded in tap water, with an initial temperature of 21.5°C. The water used in these experiments was stored in an open container and exposed to a surrounding temperature of 22°C and an increase of 0.5°C was measured in the water temperature during the high cycle fatigue measurements of more than 10^4 s.

In figure 5.3(a) the results are shown for the predictions by the 3D-constitutive model in MARC. The relation observed shows similar linearity as the creep life predictions on annealed samples in figure 2.8(b). The predictions of the low cycle fatigue prove accurate compared to the experimental results shown in figure 5.3(a). However the predictions by MARC prove accurate, it has to be noticed that the predictions are not corrected for the difference in temperature of 0.5°C for the low cycle fatigue.

The limitations of the current MARC implementation (isothermal and no influence of ageing) and the time needed for the computations, make it attractive to find an alternative for MARC to do the rest of the simulations. In the measurements performed in this study only uniaxial loading conditions are regarded. The mathematical program Matlab is used to convert the code for uniaxial conditions and to perform simulations. Since the code is now manually adjustable, it can be adjusted to take into account ageing and temperature.

The contributions of the hardening stress and driving stress were split in equation 2.1. The contribution of the hardening stress on the total stress applied is approximately 1 MPa (±0.2 MPa) for the

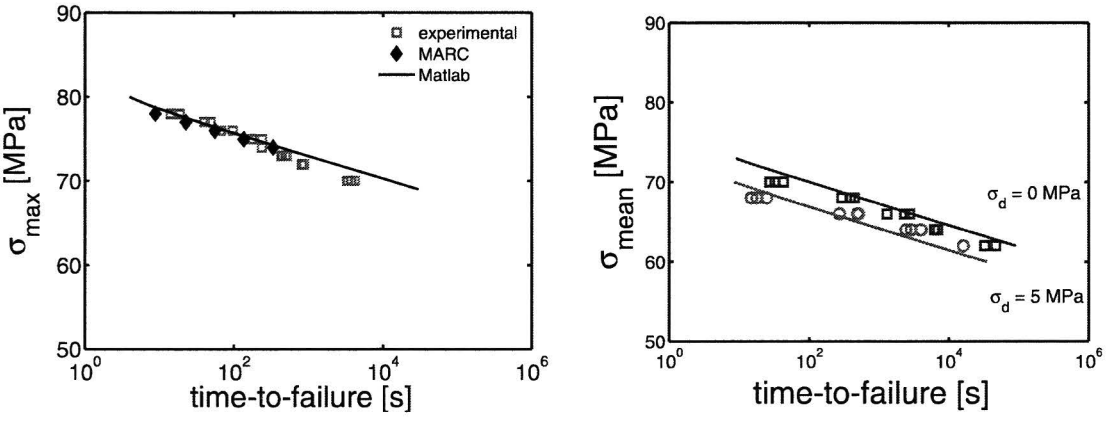

Figure 5.3: *Predictions in MARC (diamonds) and Matlab (solid line) compared with the experimental results (circles) of the fatigue life of Lexan* $101R$*, with a* S_a *of* 43.6*, for a large stress amplitude signal (a). Predictions (lines) and experimental results (symbols) for Lexan* $161R$*, with a* S_a *of* 42.4*, for a small stress amplitude signal (b).*

maximum stresses used in the experiments. The hardening stress is ignored in the simulations since the contribution is considered small and saves computation time. In the uniaxial modelling only the accumulated plastic strain as a function of the viscosity and stress is taken into account.

Ductile failure under constant loading was shown by Klompen et al. [2] to originate from the true strain softening. The softening was defined as a function solely depending on the accumulated plastic strain. The viscosity is again defined in equation 5.1 and 5.2.

$$\eta\left(T,S,\bar{\tau},p\right) = \eta_{0,r}\left(T\right)\cdot\frac{\left(\bar{\tau}/\tau_0\right)}{\sinh\left(\bar{\tau}/\tau_0\right)}\exp\left(\frac{\mu p}{\bar{\tau}_0}\right)\exp\left(S\right) \tag{5.1}$$

$$\eta_{0,r}\left(T\right) = A_{0,r}\tau_0\exp\left(\frac{\Delta U}{R}\left(\frac{1}{T}-\frac{1}{T_{ref}}\right)\right) \tag{5.2}$$

In uniaxial tensile conditions the hydrostatic pressure (p) is defined by

$$p = -\frac{\bar{\tau}}{\sqrt{3}} \tag{5.3}$$

In combination with the definition for the viscosity in equation 5.1 and the zero-viscosity in equation 5.2, this equivalent plastic strain rate for uniaxial loading conditions can be written as

$$\dot{\bar{\gamma}}\left(\bar{\tau},T,S\right) = \frac{1}{A_0}\sinh\left(\bar{\tau}/\tau_0\right)\exp\left(\frac{\mu\bar{\tau}}{\sqrt{3}\tau_0}\right)\exp\left(-\frac{\Delta U}{R}\left(\frac{1}{T}-\frac{1}{T_{ref}}\right)\exp\left(-S\right)\right. \tag{5.4}$$

The S_a-values used in the simulations in Matlab are adapted from the MARC simulations of the tensile tests and are not corrected for the negligence of the strain hardening. In figure 5.3(a) is shown that

even with the simplified uniaxial model representation the predictions of the time to failure remain accurate. In figure 5.3(b) the results are shown for an other wave-form represented in figure 3.1(c), with a small stress amplitude of 5 MPa. As well for the large stress amplitude signal as for the small stress amplitude signal the predictions are accurate. A small overprediction for the long-term creep is observed in the results in figure 5.3(b) as was also observed in figure 5.3(a).

The deviation on the short-term creep and fatigue is explained by the high stresses, close to the yield stress where heating of the sample has to be regarded for the fatigue loadings. On the short- and long-term the deviation between fatigue life predictions and measurements is explained most probably by negligence of the strain hardening in the model. When the approximated influence of the strain hardening of approximately 1 MPa is taken into account, the predicted time to failure is again accurate compared to the experimental results. In the experimental results the influence of the temperature is minimised, but can not be excluded completely for stresses close to the yield stress.

5.2 Predictions on the ageing kinetics

The ageing of the material has been shown to strongly influence the deformation behaviour of polycarbonate. The decrease of dissipated energy, the increase of the yield stress and the transition of ductile failure to brittle failure of the samples are all observed in the experiments and induced by the ageing of the material [2, 10, 11]. Klompen et al. [1, 2] described the evolution of the yield stress in time as a function of the effective time as was also shown in section 2.2.

$$\sigma_y(t) = \sigma_{y,0} + c \cdot \log\left(\frac{t_{eff} + t_a}{t_0}\right) \tag{5.5}$$

where $\sigma_{y,0}$ is 23.4 MPa and c is 3.82 MPa for polycarbonate. The influence of stress and temperature are captured in the effective time and influence the evolution of the yield stress by acceleration of the evolution time.

$$t_{eff}(T, \bar{\tau}, t) = \int_0^t \frac{d\xi}{a_T(T(\xi)) \cdot a_\sigma(\bar{\tau}(\xi))} \tag{5.6}$$

The shift factors for the temperature (a_T) and the stress (a_σ) were defined in equation 2.18.

The effective time uses a temperature and a stress activated shift factor to include the effect of temperature and stress in the model in analogy with the viscosity as shown in section 2.2. The definition of the evolution of the yield stress has not yet been validated for cyclic loading conditions. Yee et al. [21] stated physical ageing and fatigue ageing to be two individual processes. In this study the assumption is made that the physical ageing and fatigue ageing are a single proces and can be described by the relation as provided in equation 5.5. The integral in the definition of the effective time is approximated by a sum of small time-steps, with constant values for the temperature and the stress over a time period of one second.

To investigate the ageing under dynamic stress loadings and to validate the prediction of the yield stress evolution, the yield stress is measured for samples after fatiguing them for a specific number of cycles as shown in figure 5.4. In figure 5.4(a) and figure 5.4(b) the results of the yield stress measurements are shown for a large amplitude stress signal and small amplitude stress signal, respectively. Regarding

the temperature measurements in figure 4.4(b) the measurements in figure 5.4(a) and figure 5.4(b) are assumed not to be influence by heating of the sample. The yield stress measurements in figure 5.4(a) as well as in figure 5.4(b) are accurately predicted. In figure 5.4(c) a situation is considered where heating of the sample is expected when again the temperature measurements in figure 4.4(b) are taken into account. The prediction for the yield stress, performed for isothermal conditions, predicts an increase on larger times then measured in the experiments. The temperature data in figure 4.4(b) is used in the calculation of the effective time to take the heating of the sample into account. The prediction of the yield stress increase, corrected for the temperature increase, is shown in figure 5.4(d). The prediction of the yield stress in figure 5.4(d) improves in accuracy when the temperature is included. However, the still existing deviation between the prediction and the measurements can induce large differences in the simulations.

The relation describing the increase of the yield stress under influence of the ageing was derived by Klompen et al. [2] for low stresses. The relation is successfully used to describe the ageing under cyclic loading conditions, but has not been validated yet for use with high stresses. A study to validate the description of the ageing under high stresses is needed to further improve the description of ageing during fatigue.

The prediction of the ageing is included to the simulation program in Matlab. Quenched samples of polycarbonate are used to validate the predicted ageing in fatigue lifetime predictions. In figure 5.5(a) the results are shown for measurements with a small amplitude stress signal.

Concerning only the fatigue lifetime predictions, the predictions in figure 5.5(a) for the amplitude of 5 MPa shows a small deviation between experimental results and predictions. A part of the deviation is explained by neglecting the strain hardening which shifts the prediction to shorter lifetimes. Also visible in figure 5.4(a) is that the prediction of ageing stays behind on the measurements. In figure 5.5(b) the results for the large amplitude stress signal show a small deviation for the short-term predictions, but the deviation increases for larger times. The large deviation between the prediction and the experiments can not be fully explained. The prediction of the lifetime in figure5.5(b) gives no evidence of a gradual slopes change that is usually observed for ageing [2]. The prediction shows only a slight tendency of ageing at 10^4 s. This is however in accordance with the results in figure 5.4(c), where it was seen that the ageing started earlier in the experiments than predicted. The measured yield stress started to increase at 10^2 s while an increase was predicted to start at 10^4 s. The effect seems rather small in the prediction of the ageing, but has a large influence on the prediction of the fatigue lifetime. To see whether the difference in ageing predictions and measurements can fully explain the deviation in figure 5.5(b), measurements and simulations have to be performed for lifetimes larger than 10^6 s in order to see if the experiments and predictions comply again on larger time scales. An other solution is to redetermine the stress dependency of the ageing. Klompen et al. determined the stress dependency only for low stress up to 26 MPa while the stresses in the fatigue lifetime experiments reach up to 70 MPa and more.

In figure 5.6 the measurements of Klompen et al for the stress dependency are shown. The a small change of slope has large influence on the predictions of evolution of the the yield stress and as can be seen in figure 5.6 the determined slopes are disputable. A more intensive study is needed on this subject.

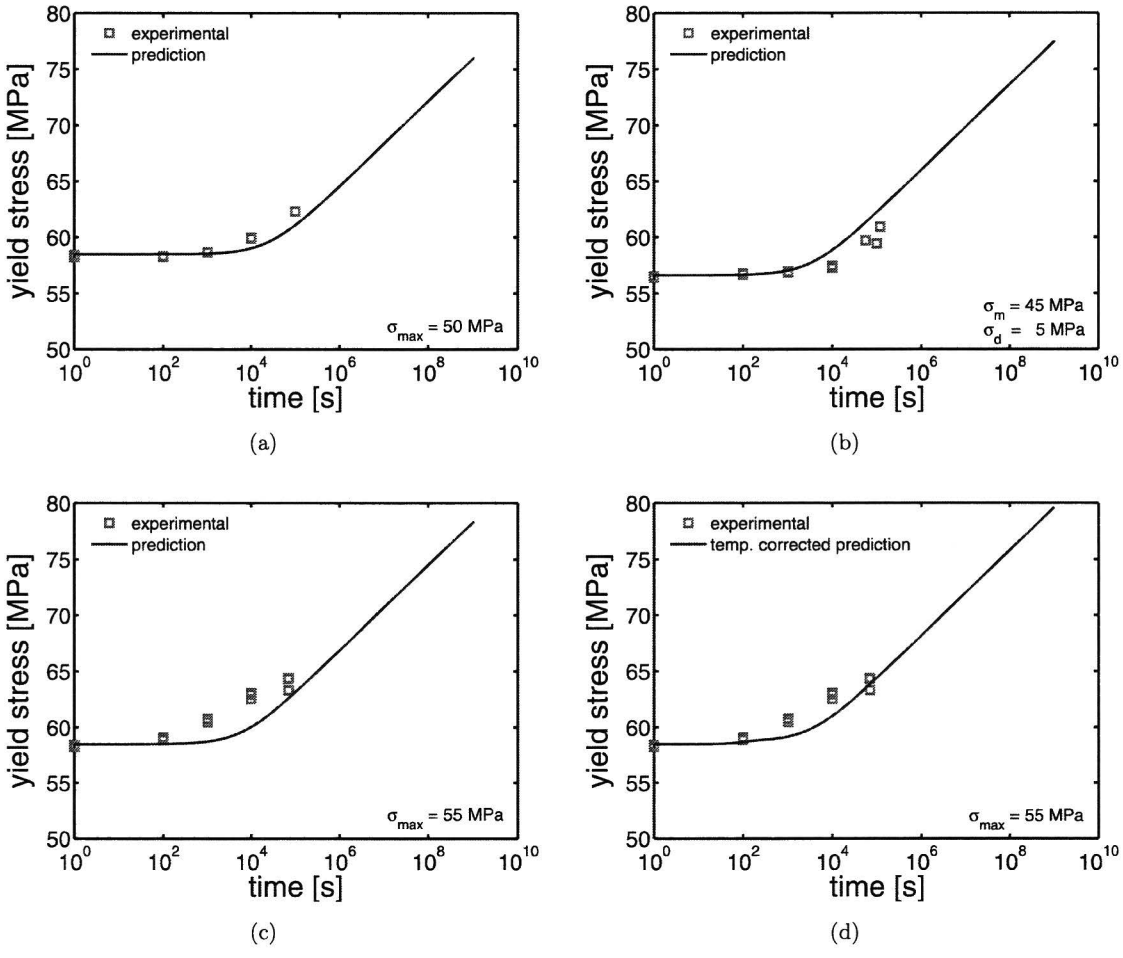

Figure 5.4: *Measurements are performed on quenched Lexan* $101R$*, with a* S_a *of* 27.3 *(a,c,d) and quenched Lexan* $161R$*, with a* S_a *of* 27.2 *(b). Predictions (lines) and experimental results (symbols) of the yield stress for Lexan* $101R$ *with a large stress amplitude (a) and Lexan* $101R$ *with a small stress amplitude (b). Isothermal (c) and non-isothermal predictions (d) for Lexan* $101R$ *for a large stress amplitude.*

5.3 Hysteretic heating

The effect of hysteretic heating on the fatigue life measurements is shown in the experimental results in chapter 4. It is widely accepted that the internal damping of the material is responsible for the temperature increase [14, 28–34]. Hence, an estimate of the dissipated energy and the initial temperature increase can be obtained from the materials loss compliance as shown earlier. The work inserted to the material by subscribing a stress signal, can be written as

$$\mathrm{W} = \int \sigma d\varepsilon \tag{5.7}$$

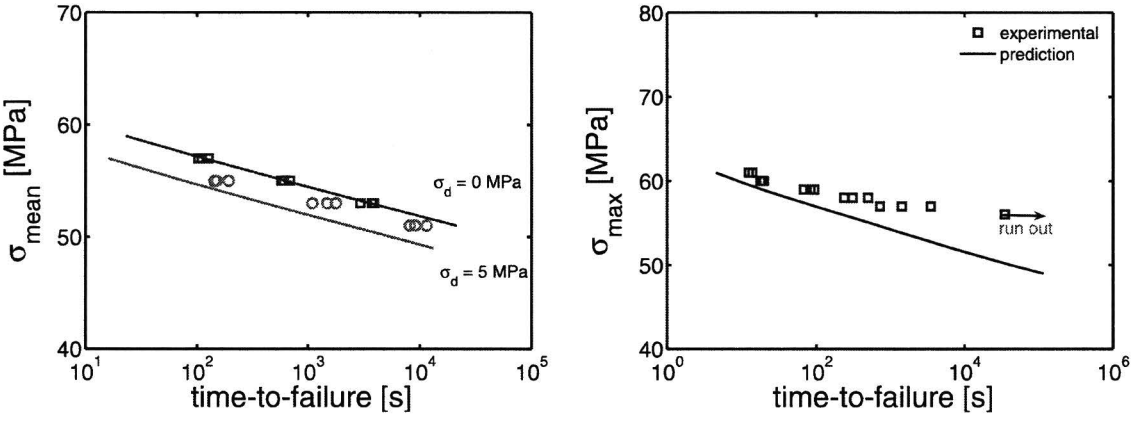

(a) (b)

Figure 5.5: *Measurements are performed on quenched Lexan* $101R$*, with a* S_a *of* 29.7 *(a) and quenched Lexan* $101R$*, with a* S_a *of* 27.3 *(b). Fatigue lifetime predictions (lines) and experimental results (symbols) for quenched Lexan* $101R$*, using a sawtooth shaped stress signal with a small amplitude (a) and Lexan* $101R$ *using a sine shaped stress signal with a large amplitude (b). Run out: no failure during the time of measurement.*

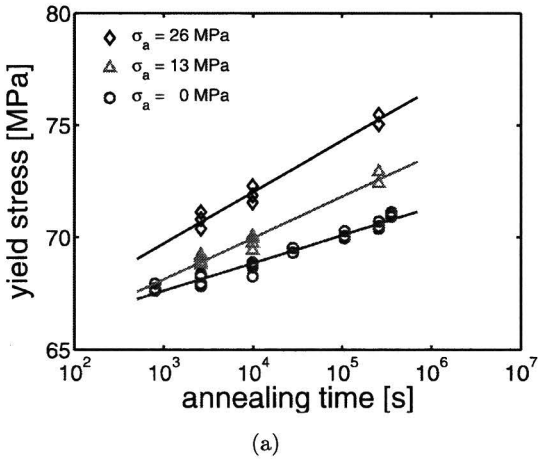

(a)

Figure 5.6: *The evolution of the yield stress as a function of annealing time for different constant stresses at* 80° *C. Figure is adapted from Klompen et al. [9]*

The strain is a function of the stress and the compliance of the material

$$\varepsilon(t) = \sigma(t) D(t) \tag{5.8}$$

It can be shown that the work inserted to the material per cycle for a sine shaped stress signal of the form

$$\sigma(t) = \sigma_m + \sigma_d \cdot \sin(\omega t) \tag{5.9}$$

where σ_m is the static stress and σ_d is the stress amplitude, can be written as where D_d is the dynamic compliance of the material.

$$W = \int_0^{\frac{2\pi}{\omega}} (\sigma_m + \sigma_d \cdot \sin(\omega t)) \cdot (\omega D_d \sigma_d \cos(\omega t - \delta))\, dt \tag{5.10}$$

where ω is the angular speed, D_d is the dynamic compliance of the material and δ is a shift in the phase taking into account the difference between the prescribed stress signal and the true strain respons. The equation can be rewritten to

$$W = \pi \sigma_d^2 D" \tag{5.11}$$

where $D"$ is the loss compliance ($D" = D_d \sin(\delta)$) and the work per cycle is a function of the stress amplitude and the loss compliance.

The rate of energy dissipation and temperature increase are now given by

$$\frac{dQ}{dt} = f \pi \sigma_d^2 D''(f, T, t) \tag{5.12}$$

$$\frac{dT}{dt} = \frac{dQ}{dt} \cdot \frac{1}{c_p \rho} \tag{5.13}$$

where Q is the dissipated energy, T the absolute temperature, $D"$ the loss compliance, c_p the heat capacity, ρ the material density and f the frequency.

The loss compliance is defined as a function of the angular speed, temperature and time. The retardation times used in the definition of the loss compliance must be obtained experimentally for every single condition. Klompen et al. [9] described the nonlinear viscoelastic behaviour of polycarbonate by a relaxation and retardation time spectrum, listed in appendix E. The relaxation and retardation time spectrum were obtained from measurements on Lexan 161R samples, with a S_a-value of 28.3. It should be stressed that the relaxation and retardation time spectra depend on the processing history and temperature [3, 35].

In this study the retardation time spectrum of Klompen et al. [9] is used to predict the initial temperature increase during fatigue. To adapt the retardation time spectrum from table E.2, the retardation times have to be adjusted for the processing history of the material simulated.

A retardation time (τ) is generally defined as

$$\tau = \frac{1}{\eta D} \tag{5.14}$$

where D is the compliance and η is the viscosity.

Polycarbonate only shows linear viscoelastic deformation behaviour for approximately the first percentage of strain [35]. Therefore, the viscoelastic behaviour of polycarbonate is in this study described by nonlinear deformation behaviour. In chapter 2 is explained how the viscosity in the constitutive model is adjusted to describe deformation behaviour for different stresses, temperatures and processing histories. Hence, the assumption is made that the same shift factors can be used to adjust the viscosity in the definition of the retardation time for stress and temperatures during the simulation as shown in equation 5.15.

$$\tau_i(\sigma) = \tau_i(S_{a,r}) \frac{\sinh(\sigma/\sigma_0)}{(\sigma/\sigma_0)} \exp\left(\frac{\Delta U}{R}\left(\frac{1}{T} - \frac{1}{T_{ref}}\right)\right) \exp(S_a) \tag{5.15}$$

where $\tau_i(S_{a,r})$ is the retardation time corrected for the difference in age compared to the reference material.
The stress dependent shift factor is defined with a different characteristic stress ($\sigma_0 = 1.334$ [MPa]). Only the state parameter is used for the viscosity since the rejuvenation is not taken into account by the model, but can be added under comparable assumptions. Also a factor is used to correct the initial age of the material for differences in processing histories between the spectrum and the material simulated as shown in equation 5.16.

$$\tau_i(S_{a,r}) = \tau_i \cdot \exp(\Delta S_a) \tag{5.16}$$

where ΔS_a is the difference in state parameters. The state parameter for the retardation time spectrum was determined with the yield stress information reported by Klompen et al. [9]. The retardation times are assumed to be equally influenced by temperature, stress and processing history.This is again an assumption, since it was shown by Venditti et al. [36] that local differences in the influence can be shown.

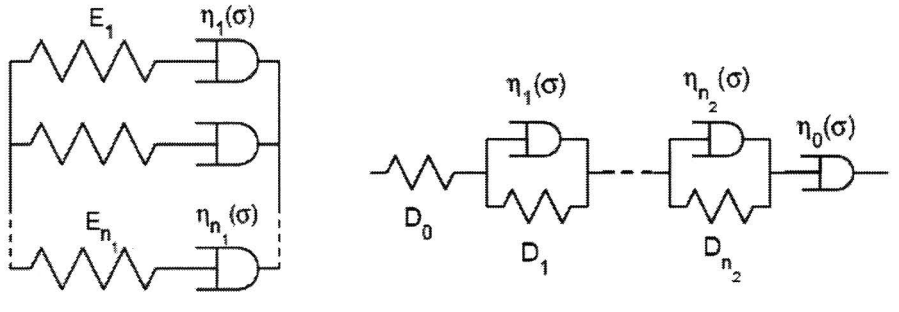

(a) (b)

Figure 5.7: *Schematic representations of the generalized nonlinear Maxwell (a) and generalized Kelvin-Voigt model (b).*

The constitutive model used for fatigue lifetime predictions uses a single mode representation of the pre-yield deformation behaviour. The pre-yield behaviour is described fully elastic and to describe nonlinear viscoelastic deformation behaviour a different model has to be used. The viscoelastic deformation of polycarbonate is simulated by use of a Maxwell and Kelvin-Voigt modulation. The

schematic, general representations of the models are shown in figure 5.7. The Maxwell model is used to describe relaxation behaviour for prescribed strains and the Kelvin-Voigt model for retardation under prescribed stresses. The Maxwell model is only used in this study for validation of the model implementation by comparing experimental results of tensile tests adapted from Klompen et al. [9] with tensile test simulations. The Kelvin-Voigt model is used to perform temperature increase predictions. The modelling is explained using the Kelvin-Voigt model as an example. The Boltzmann single integral representation in equation 5.17 is used for the description of the nonlinear viscoelastic deformation behaviour in the Kelvin-Voigt model.

$$\varepsilon(t) = \int_{-\infty}^{t} D(t - t')\, \dot{\sigma}(t')\, dt' \tag{5.17}$$

where $D(t)$ is the creep compliance defined by equation 5.18.

$$D(t) = D_0 + \sum_{i=1}^{m} D_i \left[1 - \exp\left(-\frac{t}{\tau_i}\right)\right] + \frac{t}{\eta_0} \tag{5.18}$$

where D_0 is the initial elastic respons and η_0 is the zero-flow viscosity. The index i refers to the number of the element as indexed in table E.2.

To take into account the nonlinear behaviour, the creep compliance is rewritten as shown in equation 5.19, to a stress dependent relation as was shown in chapter 2 for the viscosity.

$$D(t) = D_0 + \sum_{i=1}^{n} D_i \left[1 - \exp\left(-\frac{t}{\tau_i(\sigma)}\right)\right] + \frac{t}{\eta(\sigma)} \tag{5.19}$$

where $\tau_i(\sigma)$ ($\tau_i(\sigma) = \tau_i\, a_\sigma(\sigma)$) is the stress dependent retardation time and $\eta(\sigma)$ ($\eta(\sigma) = \eta_o\, a_\sigma(\sigma)$) is the stress dependent viscosity.

The Boltzmann integral calculations are expensive in computation time and memory. In accordance with the analogy of time-stress superposition [3, 13], a stress-reduced time is introduced in equation 5.20.

$$\psi = \int_{-\infty}^{t} \frac{dt''}{a_\sigma[\sigma(t'')]} \tag{5.20}$$

with the strain definition now rewritten to

$$\varepsilon(t) = \int_{-\infty}^{t} D(\psi - \psi')\, \dot{\sigma}(t')\, dt' \tag{5.21}$$

The integrals over the stress rate is approximated by a sum of discrete time-steps. The accuracy of the implementation is checked by simulating tensile tests performed by Klompen et al. [9]. Figure 5.8 shows the simulations with the Maxwell model for four strain rates in comparison with experimental results. The simulations and experimental data correspond for all strain rates.

The Kelvin-Voigt model is used to predict the nonlinear deformation behaviour of polycarbonate under isothermal conditions. The hysteresis loops predicted by the model for a prescribed stress signal are

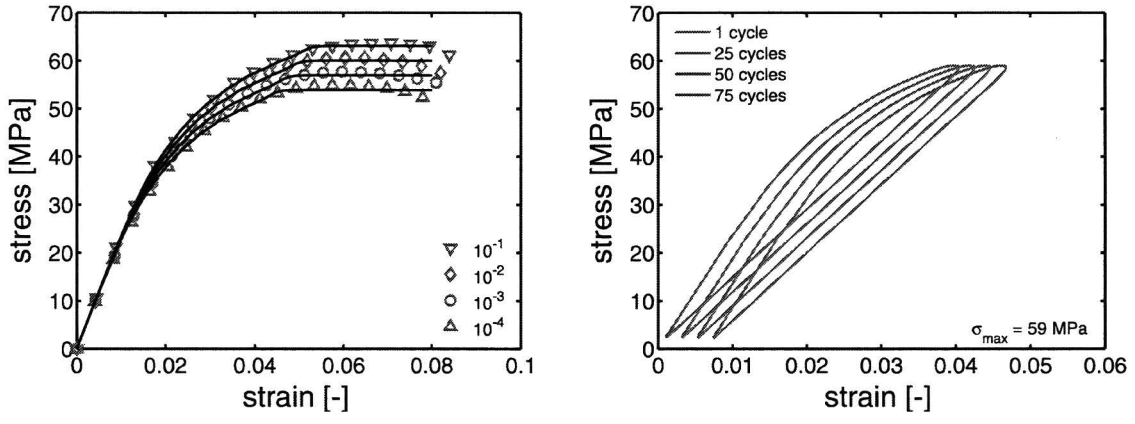

(a) (b)

Figure 5.8: *Tensile tests on Lexan 161R for different strain rates. Model prediction (solid lines) compared to experimental results (symbols) (a). The hysteretic loops for polycarbonate with a S_a of 29.5 predicted by the Kelvin-Voigt model (b)*

used to calculate a temperature increase. The hysteresis loops in the simulation show a development of the hysteresis loops over the first cycles. When a steady state is reached in the size of the hysteresis loops, the dissipated energy is calculated and a temperature increase is determined.

In figure 5.9 the results are presented for the initial temperature increase deducted from the simulations with the Kelvin-Voigt model and the results from infrared measurements. The temperature measurements are averaged values of the temperature increase over the first 20 seconds. In figure 5.9(a) the results are shown for 3 mm thick Lexan 141R samples for two different processing histories. The simulations for both series of Lexan 141R samples, show a higher temperature increase than observed in the infrared temperature measurements. An likely explanation is the low conductance of the material retarding the temperature increase of the surface of the sample. Overall the differences between simulation and experimental results are relatively small.

The shift in the two predictions of the temperature increase in figure 5.9(a) is solely determined by the way the state parameter is included in the model. By the addition of the state parameter in the definition of the viscosity contribution in the retardation time, the shift in the predictions complies with the shift observed in the experimental results.

In figure 5.9(b) the results of the temperature increase predictions and measurements are shown for the 1 mm thick Lexan 101R samples. The two series of Lexan 101R samples have different processing histories. A deviation between experimental results and predictions is observed. Noticeable is the under-prediction for the temperature increase of Lexan 101R with a S_a of 27.3 compared to the experimental results. The shift between the different processing histories is equal for as well the predictions as the experiments.

Despite the relative small differences between temperature increase predictions and measurements, the differences are to large for use in high cycle fatigue simulations. To improve the temperature increase

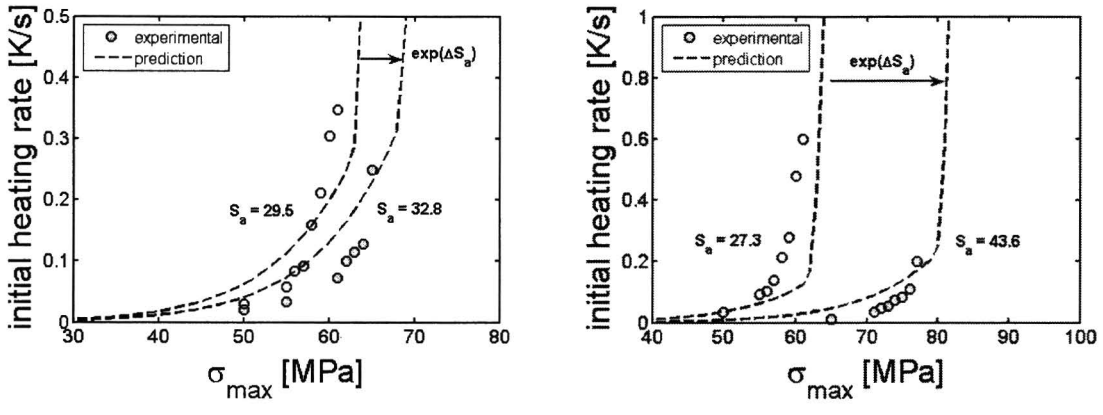

Figure 5.9: *Predictions (lines) and infrared measurements (symbols) of the initial temperature increase for Lexan* $141R$ *(a) and Lexan* $101R$ *(b) under cyclic loading.*

predictions, the description of viscoelastic deformation behaviour of polycarbonate has to be further developed.

5.4 Non-isothermal fatigue lifetime predictions

In review, it has been shown that the stress, temperature and processing history play an important role in the determination of the fatigue lifetime. The influences have been regarded individually in this study, but have not yet all three been combined in a fatigue lifetime prediction. On the other hand, the constitutive model is capable of combined predictions. Since temperature increase predictions are considered not accurate enough, the capabilities of the model are shown not on basis of a predicted temperature increase, but a temperature increase prescribed by infrared temperature measurements. A temperature profile is prescribed as function of time and kept constant at the last temperature value for the times longer than the time used to obtain infrared measurements. The simulations are performed for the isothermal and non-isothermal experiments for Lexan 101R, with S_a values of 43.6 and 27.3, as the experimental results were shown in figure 4.6.

In figure 5.10(a) the results are shown for the quenched polycarbonate. The non-isothermal fatigue lifetime predictions show equal trends compared to the experimental data, but the ageing of the material stays behind on the experiments as was discussed earlier. In figure 5.10(b) the non-isothermal predictions for annealed polycarbonate are shown. The isothermal and non-isothermal predictions enclose accurately the area with as well the isothermal measurements as the non-isothermal measurements. The results show that taking into account the temperature in the simulations can provide accurate fatigue lifetime predictions.

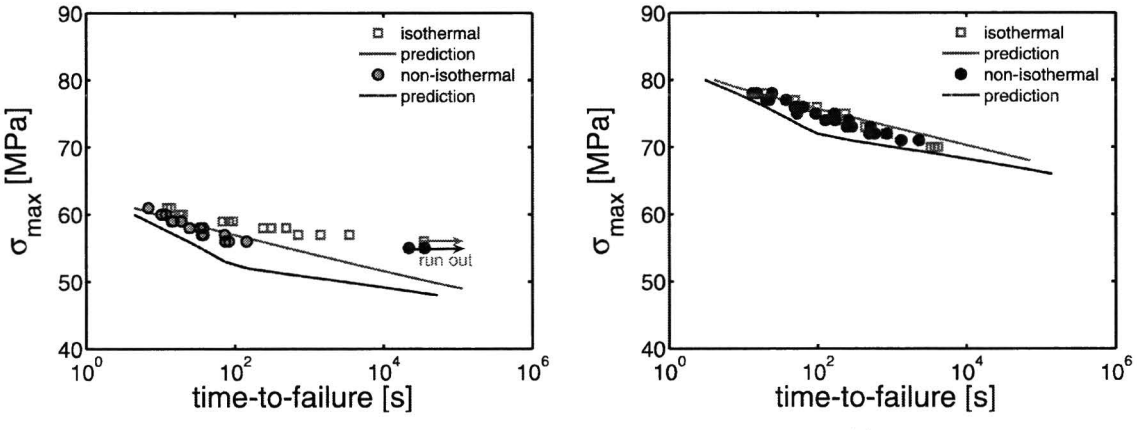

Figure 5.10: *Fatigue lifetime predictions (lines) and experimental measurements (symbols) for quenched ($S_a = 27.3$)(a) and annealed ($S_a = 43.6$)(b) Lexan 101R, with the influences of ageing and heating taken into account in the predictions. Run out: no failure during the time of measurement.*

Chapter 6

CPU-time friendly method for fatigue lifetime prediction

The goal of this study was to accurate predict the fatigue life of polycarbonate. As was shown in chapter 5 accurate fatigue life predictions were made for annealed polycarbonate under isothermal conditions. It was also observed that the simulations were consuming expensive memory and CPU-time. To reduce the CPU-time only uniaxial loading conditions were simulated. In this chapter a more efficient method is searched for to perform fast fatigue lifetime predictions in FEM-programs.

Klompen et al. [2] proved the fatigue failure to be determined by the accumulation of plastic strain. The moment of failure is the moment the material shows catastrophic localisation due to softening. The softening is triggered by a critical value of the accumulated plastic strain. Three parameters influence the accumulation of plastic strain: stress, temperature and processing history. When all three parameters are considered as a function of time, the prediction of the fatigue lifetime becomes very complex. Therefore, the conditions used in this chapter are again simplified conditions. Regarded are isothermal conditions and conditions where the ageing of the material does not have to be taken into account. Also only uniaxial loading conditions will be studied.

The plastic strain rate and the lifetime under static loadings are influenced equally by the stress as is shown in figure 6.1. The relation between the yield stress and the strain rate in figure 6.1(a) has a slope (C_α) that complies to the slope ($-C_\alpha$) of the relation between the applied stress and the time to failure in figure 6.1(b). Hence, a shift in the relation between the yield stress and the plastic strain rate will lead to an equal shift in the relation between the applied stress and the lifetime of the material.

In the previous chapter the plastic strain rate for uniaxial loadings was defined as

$$\dot{\bar{\gamma}}\left(\bar{\tau}, T, S\right) = \frac{1}{A_{0,r}} \sinh\left(\bar{\tau}/\tau_0\right) \exp\left(\frac{\mu\bar{\tau}}{\sqrt{3}\tau_0}\right) \exp\left(\frac{\Delta U}{R}\left(\frac{1}{T} - \frac{1}{T_{ref}}\right)\right) \exp\left(-S\right) \tag{6.1}$$

where μ is the pressure dependency, $A_{0,r}$ is a constant concerning the jump-frequency, τ_0 is the characteristic stress, R is the gas constant, T the absolute temperature and ΔU the activation energy.

The stress is at all times much larger compared to the characteristic stress. The hyperbolic sine in the definition of the plastic strain rate can therefore be approximated by an exponential function shown in equation 6.2.

$$\sinh\left(\frac{\bar{\tau}}{\tau_0}\right) \approx \frac{1}{2} \exp\left(\frac{\bar{\tau}}{\tau_0}\right) \tag{6.2}$$

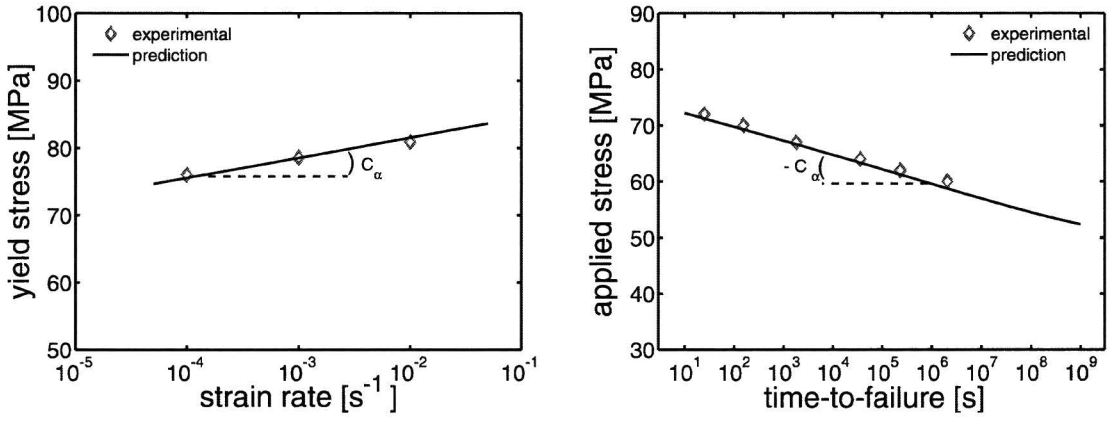

(a) (b)

Figure 6.1: *The yield stress in relation to the strain rate (a) and the applied stress in relation to the time to failure (b) for annealed polycarbonate. Figures are adapted from Klompen et al. [2]*

The definition of the plastic strain rate is rewritten to equation 6.3.

$$\dot{\bar{\gamma}}\left(\bar{\tau}\right) = \frac{1}{2A_{0,r}} \exp\left(\frac{\left(\sqrt{3}+\mu\right)\bar{\tau}(t)}{\sqrt{3}\tau_0} - \frac{\Delta U}{RT} - S\right) \tag{6.3}$$

The lifetime is determined from the accumulation of plastic strain per cycle. For a static stress ($\bar{\tau}_m$) the accumulated plastic strain ($\Delta\bar{\gamma}_s$) can be defined as

$$\Delta\bar{\gamma}_s\left(\bar{\tau}_m\right) = \frac{1}{2A_{0,r}} \cdot \exp\left(\frac{\left(\mu+\sqrt{3}\right)\cdot\bar{\tau}_m}{\sqrt{3}\tau_0} + \frac{\Delta U}{RT} - S\right) \tag{6.4}$$

with f the frequency.

By use of equation 6.4 it is now easy to calculate the number of cycles needed to obtain a critical value for the accumulated plastic at which the material will fail. The same can be done for a cyclic stress signal. An arbitrary stress signal can be written as a constant stress complemented with a dynamic stress contribution as shown in equation 6.5.

$$\bar{\tau}\left(t\right) = \bar{\tau}_m + \bar{\tau}_d \cdot \zeta\left(f,t\right) \tag{6.5}$$

where $\bar{\tau}_m$ is the mean stress, $\bar{\tau}_d$ is the stress amplitude of the dynamic stress signal and ζ is a function of frequency and time, describing the shape of the dynamic stress contribution.

The split in stress contributions in equation 6.5 allows equation 6.3 for a cyclic stress signal to be rewritten. In the new definition of the accumulated plastic strain per cycle for a cyclic stress signal ($\Delta\bar{\gamma}_{sd}$) a formulation is derived, where the static and dynamic contributions are taken apart as shown in equation 6.6.

$$\Delta\bar{\gamma}_{sd}\left(\bar{\tau}\left(t\right)\right) = \Delta\bar{\gamma}_{s}\left(\bar{\tau}_{m}\right) \cdot \int_{0}^{1} \exp\left(\frac{\left(\mu+\sqrt{3}\right)\bar{\tau}_{d}\cdot\zeta\left(f,t\right)}{\sqrt{3}\tau_{0}}\right)dt \tag{6.6}$$

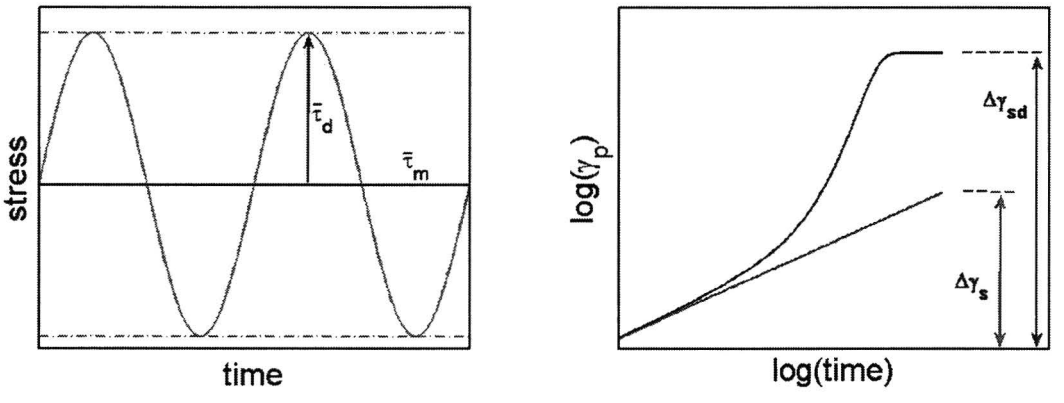

(a) (b)

Figure 6.2: *Schematic representation of the stress signals used (a). The accumulation of plastic strain over the period of a single cycle for a static ($\Delta\bar{\gamma}_s$) and a sine shaped, dynamic ($\Delta\bar{\gamma}_{sd}$) stress signal (b).*

In equation 6.6 it becomes clear how the dynamic stress contribution can be regarded as an acceleration factor on the accumulated plastic strain induced by the static stress contribution. The difference between the two accumulated plastic strains is for a single period schematically represented in figure 6.2. In figure 6.2(b) the shape of the curve of $\Delta\bar{\gamma}_{sd}$ can change for differences in for example phase, frequency, amplitude and shape of the dynamic stress signal.

The dynamic stress contribution has been presented as an time-dependent factor on the plastic strain accumulated under static stress conditions. The suggesting is made that a fast creep lifetime prediction can be shifted to fatigue lifetime predictions by a single acceleration factor determined by the difference in accumulated plastic strain over the two stress signals. The acceleration factor will be defined as the rate between the accumulated plastic strains over a single cyclic stress period as represented by equation 6.7.

$$a_{\sigma d} = \frac{\int_{0}^{t} \dot{\bar{\gamma}}\left(\bar{\tau}\left(t\right)\right)dt}{\int_{0}^{t} \dot{\bar{\gamma}}\left(\bar{\tau}_{m}\right)dt} = \frac{\Delta\bar{\gamma}_{sd}}{\Delta\bar{\gamma}_{s}} \tag{6.7}$$

The acceleration factor is defined such that it shifts the lifetime predictions of any shape of cyclic stress to predict any other shape of stress as long as isothermal conditions are considered and physical ageing does not play a role in the process. A sawtooth shaped stress signal is used in appendix D as an example since it can be analytically solved. A relation for the shift of time to failure by the dynamic stress onset is derived. By working out the equation 6.7 as shown in appendix D, the acceleration factor for a sawtooth shaped stress signal is defined by

$$a_{\sigma d} = \left(\frac{\sqrt{3}\tau_0}{2\bar{\tau}_d \left(\mu + \sqrt{3}\right)} \right) \cdot \sinh \left(\frac{\left(\mu + \sqrt{3}\right) \bar{\tau}_d}{\sqrt{3}\tau_0} \right) \tag{6.8}$$

The acceleration factor for a block shaped stress signal can also be solved analytically and is defined by

$$a_{\sigma d} = \cosh \left(\frac{\left(\mu + \sqrt{3}\right) \bar{\tau}_d}{\sqrt{3}\tau_0} \right) \tag{6.9}$$

A sine shaped stress signal can not be analytically solved and has to be approximated numerically. In figure 6.3 the numerical approximation for the sine shaped stress signal is compared to the two other stress signals. In figure 6.3(b) a schematic representation is shown for the effect of the acceleration factor. The acceleration factors for 5 and 10 MPa for a sine shaped stress signal from figure 6.3(a) shift the creep lifetime predictions to shorter times as shown in figure 6.3(b). Predictions are found for fatigue lifetimes for a stress signal with the mean stress equal to the static stress used for the creep lifetime predictions and a sine shaped stress contribution around the static stress as shown for a large amplitude in figure 6.2(a). The same can be done for two complete different stress signals, but is not shown in this study.

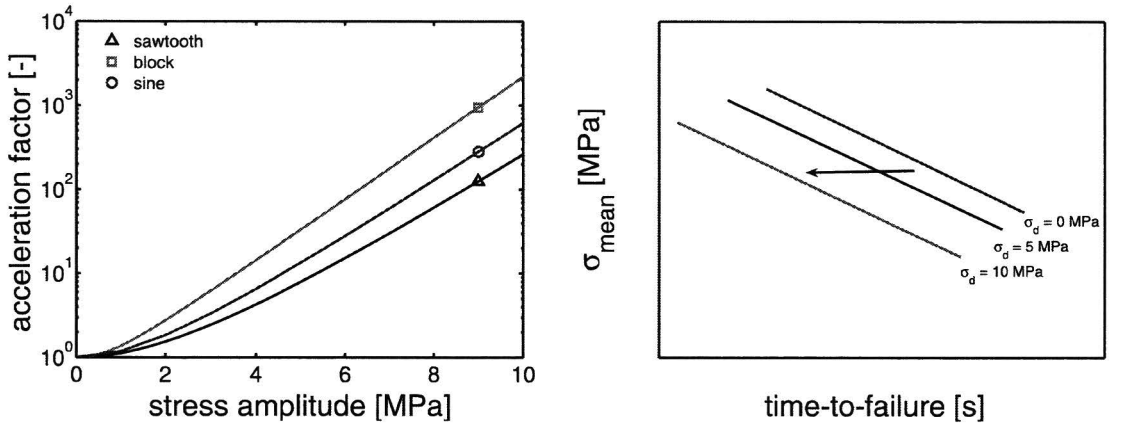

(a) (b)

Figure 6.3: *Acceleration factors to shift creep lifetime predictions to fatigue lifetime predictions (a). A schematic representation of the effect of the acceleration factor on the creep lifetime predictions to obtain fatigue lifetime predictions (b).*

The acceleration factor demands isothermal conditions and a constant material state. Thus a condition with a high S_a is most suitable for the validation of the acceleration factor. The use of the acceleration factor makes it also possible to shift arbitrary creep simulations to arbitrary fatigue predictions. Creep simulations are performed for annealed material and for a serie of mean stresses between 65 and 75 MPa. The acceleration factor is used to predict the time to failure for the experimental data as shown in figure 4.5(a). The results presented in figure 5.6(a) show conformity between prediction and experimental results. Under the stated conditions it is proven that a simple shift factor can be used to predict fatigue lifetimes from creep lifetime predictions.

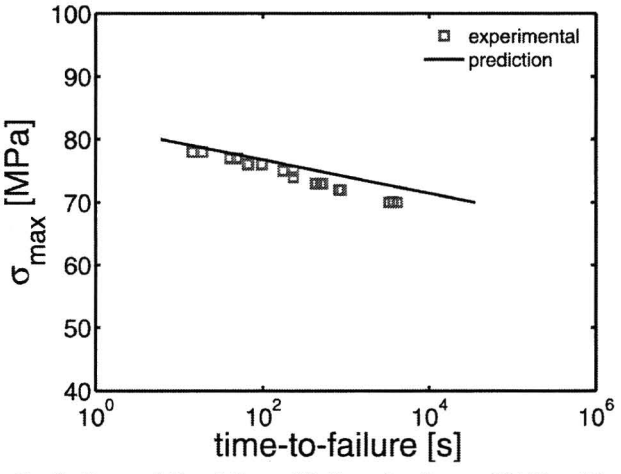

Figure 6.4: *Predictions of the fatigue lifetime for Lexan* $101R$*, with a* S_a *of* 43.6 *for a large amplitude stress stress signal, by shifting creep lifetime predictions (a).*

Conclusions and Remarks

This study concerned the fatigue failure behaviour of glassy polymers. Experiments were performed to determine the parameters that influence the fatigue life of polycarbonate. It was shown in the fatigue lifetime experiments that the fatigue failure is determined by the accumulation of plastic strain. Also three parameters were shown to influence the fatigue lifetime: stress, temperature and processing history.

The characteristics of fatigue lifetime measurements, as indicated by Lesser [14] for polyacetal, were observed in experiments on polycarbonate. The thermally and mechanically dominated regions were observed and a plateau in between the regions was noticed. The plateau was shown to be determined by the balance between heat generation in the sample and the heat loss to the surroundings. Also the transition in failure mode from necking to brittle rupture was observed in the measurements and was explained by ageing of the material. The influence of the frequency on the fatigue lifetime, as stated in the literature [18], was not observed in the experiments.

Ageing showed to increase the yield stress under fatigue loading conditions and shifted the fatigue lifetime of the polymer to larger times. The ageing was shown to be predicted accurately by the relation derived by Klompen et al. [2]. The small deviation between the prediction and the measurements proved to strongly influence the fatigue lifetime predictions. The evolution of the yield stress through ageing must be re-evaluated for use in fatigue loading conditions, since the relation was only validated for use with lower stresses.

The heating of the material was successfully measured by an infrared camera. The temperature of the material was related to the dissipated energy and was shown to be directly influenced by the increase of the yield stress through ageing. A nonlinear Kelvin-voigt model in combination with a retardation time spectrum, was used to successfully predict the rate of temperature increase of the sample during fatigue loading. The model accurately took in account the influence of the differences in processing history.

The constitutive model, developed in Eindhoven and reported on by Klompen et al. [1, 2], was applied to predict the fatigue lifetime for polycarbonate. The numerical predictions were accurate for annealed material under isothermal conditions. The predictions on quenched polycarbonate proved less accurate. Small differences between the predictions and measurements of the evolution of the yield stress due to ageing, proved to have large consequences on the fatigue lifetime predictions. A better description of the yield stress evolution can improve the fatigue lifetime predictions.

It was shown that an acceleration factor could be defined, that shifts fast creep lifetime predictions to fatigue lifetime predictions. The acceleration factor can only be defined for isothermal conditions and conditions where ageing does not occur.

References

[1] E.T.J. Klompen, T.A.P. Engels, L.C.A. van Breemen, P.J.G. Schreurs, L.E. Govaert, and H.E.H. Meijer. Quantative prediction of long–term failure of polycarbonate. *Macromolecules*, 38:7009–7017, 2005.

[2] E.T.J. Klompen, T.A.P. Engels, L.E. Govaert, and H.E.H. Meijer. Modeling of the post-yield response of glassy polymers: influence of thermomechanical history. *Macromolecules*, 38:6997–7008, 2005.

[3] E.T.J. Klompen and L.E. Govaert. Nonlinear viscoelastic behaviour of thermorheollogically complex materials. *Mechanics of Time-Dependent Meterials*, 3:49–69, 1999.

[4] O.A. Hasan and M.C. Boyce. A constitutive model for the nonlinear viscoelastic viscoplastic behavior of glassy polymers. *Polymer Engineering and Science*, 35(4):331–344, February 1995.

[5] M.C. Boyce, D.M. Parks, and A.S. Argon. Large inelastic deformation of glassy polymers. part i: Rate dependent constitutive model. *Mechanics of Materials*, 7:15–33, 1988.

[6] A.D. Mulliken and M.C. Boyce. Mechanics of the rate–dependent elastic–plastic deformation of glassy polymers from low to high strain rates. *International Journal of Solids and Structures*, 43(5):1331–1356, March 2006.

[7] C.P. Buckley and D.C. Jones. Glass-rubber constitutive model for amorphous polymers near the glass transition. *Polymer*, 36(17):3301–3312, 1995.

[8] H.E.H. Meijer and L.E. Govaert. Mechanical performance of polymer systems: The relation between structure and properties. *Progres in Polymer Science*, 30:915–938, 2005.

[9] E.T.J. Klompen. *Mechanical properties of solid polymers, Constitutive modelling of long and short term behavior.* PhD thesis, Technische Universiteit Eindhoven, 2005.

[10] J.M. Hutchinson. Physical aging of polymers. *Progressions on Polymer Science*, 20:703–760, 1995.

[11] H.G.H Van Melick, L.E. Govaert, and H.E.H Meijer. Localisation phenomena in glassy polymers: influence of thermal and mechanical history. *Polymer*, 44:3579–3591, 2003.

[12] R. Haward and G. Thackray. The use of a mathematical model to describe isothermal stress-strain curves in glassy polymers. *Proceedings of the Royal Society A*, 302:453–472, 1968.

[13] H. Leaderman. *Elastic and creep properties of filamentous materials and other high polymers.* The Textile Foundation, Washington D.C., 1943.

[14] A.J Lesser. Fatigue behavior of polymers. In *Encyclopedia of Polymer Science and Technology.* John Wiley & Sons, Inc., 2002.

[15] A.J Lesser. Changes in mechanical behavior during fatigue of semicrystalline thermoplastics. *Journal of Applied Polymer Science*, 58:869–879, 1995.

[16] A.J Lesser. Effective volume changes during fatigue and fracture of polyacetal. *Polymer Engineering and Science*, 36(18):2366–2374, September 1996.

[17] R.J. Crawford and P.P. Benham. Cyclic stress fatigue and thermal softening failure of a thermoplastic. *Journal of Materials Science*, 9:18–28, 1974.

[18] R.J. Crawford and P.P. Benham. Some fatigue characteristics of thermoplastics. *Polymer*, 16:908–914, 1975.

[19] A.F. Yee. Strain and temperature accelerated relaxation in polycarbonate. *Journal of Polymer Science: Part B: Polymer Physics*, 26:2463–2483, 1988.

[20] X. Li, A.F. Hristov, H.A. and, and D.W. Gidley. Influence of cyclic fatigue on the mechanical properties of amourphous polycarbonate. *Polymer*, 36(4):759–765, 1995.

[21] L.B. Liu, A.F. Yee, and D.W. Gidley. Effect of cyclic stress on enthalpy relaxation in polycarbonate. *Journal of Polymer Science: Polymer Physics Edition*, 30:221–230, 1992.

[22] L.C.E. Struik. The mechanical and physical ageing of semi-crystalline polymers: 1. *Polymer*, 28:1521–1533, August 1997.

[23] L.C.E. Struik. The mechanical and physical ageing of semi-crystalline polymers: 2. *Polymer*, 28:1534–1542, August 1997.

[24] T.L. Smith, G. Levita, and W.K. Moonan. Reversal and activation of physical aging by applied deformations in simple compression and extension. *Journal of Polymer Science: Part B: Polymer Physics*, 26:875–881, 1988.

[25] C. Bauwens-Crowet and J-C. Bauwens. Rejuvenation and annealing effects on the loss curve of polycarbonate: 1. structural temperature dependence. *Polymer*, 31:248–252, February 1990.

[26] C. Bauwens-Crowet and J-C. Bauwens. Rejuvenation and annealing effects on the loss curve of polycarbonate: 2. cooling and ageing dependence. *Polymer*, 31:646–650, April 1990.

[27] J.A. Koenen. Observation of the heat exchange during deformation using a infra-red camera. *Polymer*, 33(22):4732–4736, 1992.

[28] D. Rittel and Y. Rabin. An investigation of the heat generated during cyclic loading of two glassy polymers. part 2: Thermal analysis. *Mechanics of Materials*, 32:149–159, 2000.

[29] K. von Oberbach. Erwärmungsverhalten von kunststoffen bei dynamischer beanspruchung. *Kunststoffe*, 59(1):37–39, 1969.

[30] R. Kapoor and S. Nemat-Nasser. Determination of temperature rise during high strain rate deformation. *Mechanics of Materials*, 27:1–12, 1998.

[31] A. Molinari and Y. Germain. Self heating and thermal failure of polymers sustaining a compressive cyclic loading. *International Journal of Solids Structures*, 33(23):3439–3462, 1996.

[32] D. Rittel. On the conversion of plastic work to heat during high strain rate deformation of glassy polymers. *Mechanics of Materials*, 31:131–139, 1999.

[33] D. Rittel. An investigation of the heat generated during cyclic loading of two glassy polymers. part 1: Experimental. *Mechanics of Materials*, 32:131–147, 2000.

[34] T.R. Tauchert. The temperature generated during torsional oscillations of polyethylene rods. *International Journal of Engineering Science*, 5:353–365, Mid–November 1967.

[35] T.A. Tervoort, E.T.J. Klompen, and L.E. Govaert. A constitutive model equation for the elasto–viscoplastic deformation of glassy polymers. *Mechanics of Time-Dependent Materials*, 1:269–291, 1998.

[36] R.A. Venditti and J.K. Gillham. Physical ageing deep in the glassy state of a fully cured polyimide. *Journal of Applied Polymer Science*, 45:1501–1516, 1992.

Appendix A

Dissipated energy per cycle

The work inserted to the material by subscribing a stress signal, can be written as

$$\mathrm{W} = \int \sigma d\varepsilon = \int \sigma \frac{d\varepsilon}{dt} dt \tag{A.1}$$

In the experiments the material is subdued to a sine shaped stress signal that can be decomposed into a static (σ_m) and a dynamic (σ_d) stress contribution

$$\sigma(t) = \sigma_m + \sigma_d \cdot \sin(\omega t) \tag{A.2}$$

The strain is a function of the stress and the compliance of the material

$$\varepsilon(t) = \sigma(t) D(t) \tag{A.3}$$

where D_d is the dynamic compliance of the material.

Assuming a nonlinear behaviour of the material a shift in the phase (δ) takes into account the difference between prescribed stress signal and the true strain respons.

$$\varepsilon(t) = D_d(\sigma_m + \sigma_d \sin(\omega t - \delta)) \tag{A.4}$$

The derivative becomes then

$$\frac{d\varepsilon}{dt} = \omega D_d \sigma_d \cos(\omega t - \delta) \tag{A.5}$$

Leading to a full representation of the work per cycle

$$W = \int_0^{\frac{2\pi}{\omega}} (\sigma m + \sigma d \cdot \sin(\omega t)) \cdot (\omega D_d \sigma_d \cos(\omega t - \delta))\, dt \tag{A.6}$$

$$\begin{aligned} W = \; & \sigma_m \sigma_d D_d \left[\sin(\omega t)\cos(\delta) - \cos(\omega t)\sin(\delta)\right]_0^{\frac{2\pi}{\omega}} \\ & + \sigma_d^2 D_d \left[\tfrac{1}{2}\sin^2(\omega t)\cos(\delta) - \tfrac{1}{2}\cos(\omega t)\sin(\delta) + \tfrac{1}{2}\omega t\right]_0^{\frac{2\pi}{\omega}} \end{aligned} \tag{A.7}$$

$$W = \pi \sigma_d^2 D'' \tag{A.8}$$

where $D'' = D_d \sin(\delta)$

The dissipated energy per period becomes

$$\frac{dQ}{dt} = f \cdot \frac{\pi \sigma_d^2 D''}{c_p \rho} \tag{A.9}$$

where Q is the dissipated energy, f is the frequency, D'' is the loss compliance of the material, c_p is the specific heat coefficient and ρ is the density.

Appendix B

Loss compliance

The definition of the strain uses a Boltzmann single integral

$$\varepsilon(t) = \int_{-\infty}^{t} D(t-t')\dot{\sigma}(t')\,dt' \tag{B.1}$$

The compliance is defined as a function of time.

$$D(t) = D_0 + \sum_{i=1}^{n} D_i\left(1 - \exp^{\left(-\frac{t}{\tau_i}\right)}\right) + \frac{t}{\eta_0} \tag{B.2}$$

The cyclic stress signal and the derivative are defined as

$$\sigma(t) = \sigma_m + \sigma_d \sin(\omega t) \tag{B.3}$$

$$\dot{\sigma}(t) = \omega\sigma_d \cos(\omega t) \tag{B.4}$$

The strain becomes now

$$\varepsilon(t) = \int_{\tau=-\infty}^{t} D(t-\tau)\omega\sigma_d \cos(\omega\tau)\,d\tau \tag{B.5}$$

The sine shaped stress signal starts at the moment of $t = 0$

$$\varepsilon(t) = \int_{\tau=0}^{t} D(t-\tau)\omega\sigma_d \cos(\omega\tau)\,d\tau \tag{B.6}$$

Inserting the compliance function from equation B.2 gives

$$\varepsilon(t) = \int_{\tau=0}^{t} \left\{D_0 + \sum_{i=1}^{n} D_i\left(1 - \exp^{\left(-\frac{t-\tau}{\tau_i}\right)}\right) + \frac{t-\tau}{\eta_0}\right\}\omega\sigma_d \cos(\omega\tau)\,d\tau \tag{B.7}$$

This can be rewritten to

$$\begin{aligned}\varepsilon(t) = \sum_{i=1}^{n} \Bigg(& \left(D_0 + D_i + \frac{t}{\eta_0}\right)\sigma_d - \frac{\sigma_d t}{\eta_0} + \frac{D_i \exp^{\left(-\frac{t}{\tau_i}\right)} \exp^{\left(\frac{t}{\tau_i}\right)} \omega^2\sigma_d}{\frac{1}{\tau_i} + \omega^2}\Bigg)\sin(\omega t) \\ & - \left(\frac{D_i \exp^{\left(-\frac{t}{\tau_i}\right)} \exp^{\left(\frac{t}{\tau_i}\right)} \omega\sigma_d}{\tau_i\left(\frac{1}{\tau_i^2} + \omega^2\right)} + \frac{\sigma_d}{\eta_0\omega}\right)\cos(\omega t) \\ & + \left(\frac{\sigma_d}{\eta_0\omega} - \frac{1}{\tau_i\left(\frac{1}{\tau_i^2} + \omega^2\right)}\right)\end{aligned}$$

(B.8)

Using a standard formulation

$$\varepsilon(t) = \sigma_d D' \sin(\omega t) - \sigma_d D'' \cos(\omega t) + \Gamma \tag{B.9}$$

with Γ the rest term
The linear loss compliance is now defined as

$$D'' = \sum_{i=1}^{n} \left(\frac{D_i \omega \tau_i}{1 + \omega^2 \tau_i^2} + \frac{1}{\eta_0 \omega} \right) \tag{B.10}$$

Appendix C

Thermodynamics

The standard heat transfer equation can be written as [28]

$$c_p \rho \frac{dT}{dt} - k\Delta T = \frac{dQ}{dt} \tag{C.1}$$

where c_p is the specific heat coefficient, ρ the material density, T the absolute temperature, k the conduction constant and Q the dissipated energy.

The boundary condition at the wall of the sample is defined by

$$k\frac{dT}{dt} + h_c\left(T - T_0\right) = 0 \tag{C.2}$$

where h_c is the heat transfer coefficient and T_0 is the temperature of the surroundings.

The thermodynamics in this study are simplified with the assumption that conduction of heat in the sample is of no concern due to the small dimensions. The basic equation C.1 is simplified to a 1D representation of the heat transfer of the sample

$$c_p \rho \frac{dT}{dt} + h_c\left(T - T_0\right) = \frac{dQ}{dt} \tag{C.3}$$

To predict the temperature increase for experiments performed in air-temperature controlled surroundings a value for the heat transfer coefficient was taken 13.86 $[W\ K^{-1}\ m^{-2}]$, corresponding to the work of Koenen [27]. No specific value was found in literature for the heat transfer coefficient of polycarbonate in water, but an estimate was taken at the value of 100 $[W\ K^{-1}\ m^{-2}]$. The figures in figure 5.10 could be correctly reproduced using a constant initial temperature increase of the polymer as determined by the infrared temperature measurements and postulated heat transfer coefficients.

The temperature can be approximated as uniform in a sample when the Biot number is smaller enough. The Biot number is a nondimensional parameter that gives a ratio between the convection and the conduction as shown in equation C.4. A rule of thumb states a sample with a Biot number

ρ	1.22e3	$[kg/m^3]$
k	0.21	$[W\ K^{-1}\ m^{-1}]$
h_{air}	13.86	$[W\ K^{-1}\ m^{-2}]$
h_{water}	100	$[W\ K^{-1}\ m^{-2}]$
c_p	$1.3 \cdot 10^3$	$[J/kg * K]$

Table C.1: *Overview of the properties used in the heat transfer equation [28].*

smaller than 0.1 to have a uniform temperature distribution was also shown by [28]

$$B_i = \frac{hR}{k} \tag{C.4}$$

where k is the heat conductivity, h is the heat transfer constant and R is the distance of conduction. The Biot number is smaller than 0.1 for samples with a thickness of less than 3 mm [28].

Appendix D

Analytical solution accumulative plasticity

This appendix discusses the derivation of the shift factor for a sawtooth shaped stress signal. Only the steps that are crucial for this derivation are shown.

In chapter 6 the definition for the viscosity, equation D.1, was rewritten to relation for the equivalent plastic strain rate, equation D.3.

$$\eta\left(T,S,\bar{\tau},p\right)=A_{0,r}\tau_0\left(T\right)\cdot\frac{\left(\bar{\tau}/\tau_0\right)}{\sinh\left(\bar{\tau}/\tau_0\right)}\exp\left(\frac{\mu p}{\bar{\tau}_0}\right)\exp\left(\frac{\Delta U}{R}\left(\frac{1}{T}-\frac{1}{T_{ref}}\right)\right)\exp\left(S\right) \tag{D.1}$$

where μ is the pressure dependency, $A_{0,r}$ is a constant concerning the jump-frequency at a reference temperature, τ_0 is the characteristic stress, p is the hydrostatic pressure, R is the gas constant, T the absolute temperature, S the softening and ΔU the activation energy.

In this only study uniaxial loading conditions are regarded and the hydrostatic pressure (p) is therefore defined by

$$p=-\frac{\bar{\tau}}{\sqrt{3}} \tag{D.2}$$

The equivalent plastic strain rate is defined for uniaxial conditions as

$$\dot{\bar{\gamma}}\left(\bar{\tau},T,S\right)=\frac{1}{2A_{0,r}}\exp\left(\bar{\tau}/\tau_0\right)\exp\left(\frac{\mu\bar{\tau}}{\sqrt{3}\tau_0}\right)\exp\left(-\frac{\Delta U}{R}\left(\frac{1}{T}-\frac{1}{T_{ref}}\right)\right)\exp\left(-S\right) \tag{D.3}$$

The stress signal was decomposed to a static and a dynamic stress contribution as shown in equation D.4.

$$\bar{\tau}\left(t\right)=\bar{\tau}_m+\bar{\tau}_d\cdot\zeta\left(f,t\right) \tag{D.4}$$

where $\bar{\tau}_m$ is the mean stress, $\bar{\tau}_d$ is the stress amplitude of the dynamic stress signal and ζ is a function of frequency (f) and time, describing the shape of the dynamic stress contribution.

By integrating the function over the time an analytical solution can be derived for the accumulated plastic strain for the static stress signal

$$\Delta\bar{\gamma}_s\left(\bar{\tau}_m\right)=\frac{1}{2A_{0,r}}\cdot\exp\left(\frac{\left(\mu+\sqrt{3}\right)\cdot\bar{\tau}_m}{\sqrt{3}\tau_0}-\frac{\Delta U}{R}\left(\frac{1}{T}-\frac{1}{T_{ref}}-S\right)\right. \tag{D.5}$$

and for a total stress signal.

$$\Delta\bar{\gamma}_{sd}\left(\bar{\tau}\left(t\right)\right) = \Delta\bar{\gamma}_{s}\left(\bar{\tau}_{m}\right) \cdot \int_{0}^{1} \exp\left(\frac{\left(\mu+\sqrt{3}\right)\bar{\tau}_{d}\cdot\zeta\left(f,t\right)}{\sqrt{3}\tau_{0}}\right)dt \tag{D.6}$$

The acceleration factor is defined as the rate between the accumulated plastic strain under cyclic and static loading, equation D.7.

$$a_{\sigma d} = \frac{\int_{0}^{t}\dot{\bar{\gamma}}\left(\bar{\tau}\left(t\right)\right)dt}{\int_{0}^{t}\dot{\bar{\gamma}}\left(\bar{\tau}_{m}\right)dt} = \frac{\Delta\bar{\gamma}_{sd}}{\Delta\bar{\gamma}_{s}} \tag{D.7}$$

The analytical solutions for the shift factor for a sawtooth shaped stress signal and a block shaped stress signal are given in equation 6.8 and 6.9. The derivation of the analytical solution for the sawtooth shaped signal is given below as example.

To calculate the integral over the time of one period of the sawtooth shaped stress signal, the period is divided in three time parts. The integral over the whole period will be the same as the sum of the three parts.

Time interval	Definition of the stress signal ($\bar{\tau}$)
$0 \leq t < \frac{1}{4f}$	$\bar{\tau} = \bar{\tau}_{m} + 4f\bar{\tau}_{d}t$
$\frac{1}{4f} \leq t < \frac{3}{4f}$	$\bar{\tau} = \bar{\tau}_{m} + 2\bar{\tau}_{d} - 4f\bar{\tau}_{d}t$
$\frac{3}{4f} \leq t < \frac{1}{f}$	$\bar{\tau} = \bar{\tau}_{m} - 4\bar{\tau}_{d} + 4f\bar{\tau}_{d}t$

For every time interval a contribution can be calculated. For the time interval $0 \leq t < \frac{1}{4f}$ the integral can be written.

$$\Delta\bar{\gamma}_{sd} = \Delta\bar{\gamma}_{s}(\bar{\tau}_{m}) \cdot \int_{0}^{\frac{1}{4f}} \exp\left(\left(\frac{\sqrt{3}+\mu}{\sqrt{3}\tau_{0}}\right)4f\bar{\tau}_{d}t\right)dt \tag{D.8}$$

The solution for the time interval is then given by

$$\Delta\bar{\gamma}_{sd} = \Delta\bar{\gamma}_{s}(\bar{\tau}_{m}) \cdot \left(\frac{\sqrt{3}\tau_{0}}{\left(\sqrt{3}+\mu\right)4f\bar{\tau}_{d}}\right) \cdot \left(\exp\left(\left(\frac{\sqrt{3}+\mu}{\sqrt{3}\tau_{0}}\right)\bar{\tau}_{d}\right) - \exp^{0}\right) \tag{D.9}$$

In the same way a definition can be given for the time period $\frac{1}{4f} \leq t < \frac{3}{4f}$.

$$\Delta\bar{\gamma}_{sd} = \Delta\bar{\gamma}_{s}(\bar{\tau}_{m}) \cdot \exp\left(2\bar{\tau}_{d}\left(\frac{\sqrt{3}+\mu}{\sqrt{3}\tau_{0}}\right)\right)\left(\frac{\sqrt{3}\tau_{0}}{\left(\sqrt{3}+\mu\right)4f\bar{\tau}_{d}}\right) \cdot \left(\exp\left(-\bar{\tau}_{d}\left(\frac{\sqrt{3}+\mu}{\sqrt{3}\tau_{0}}\right)\right) - \exp\left(-3\bar{\tau}_{d}\left(\frac{\sqrt{3}+\mu}{\sqrt{3}\tau_{0}}\right)\right)\right) \tag{D.10}$$

and the last time period $\frac{3}{4f} \leq t < \frac{1}{f}$.

$$\Delta\bar{\gamma}_{sd} = \Delta\bar{\gamma}_s(\bar{\tau}_m) \cdot \exp\left(-4\bar{\tau}_d\left(\frac{\sqrt{3}+\mu}{\sqrt{3}\tau_0}\right)\right)\left(\frac{\sqrt{3}\tau_0}{(\sqrt{3}+\mu)\,4f\bar{\tau}_d}\right)\cdot\left(\exp\left(4\bar{\tau}_d\left(\frac{\sqrt{3}+\mu}{\sqrt{3}\tau_0}\right)\right) - \exp\left(3\bar{\tau}_d\left(\frac{\sqrt{3}+\mu}{\sqrt{3}\tau_0}\right)\right)\right) \tag{D.11}$$

The summation of the three parts will lead to

$$\Delta\bar{\gamma}_{sd} = \Delta\bar{\gamma}_s(\bar{\tau}_m) \cdot \left(\frac{\sqrt{3}\tau_0}{2\bar{\tau}_d(\sqrt{3}+\mu)}\right) \cdot \left(\exp\left(\frac{\bar{\tau}_d(\sqrt{3}+\mu)}{\sqrt{3}\tau_0}\right) - 1\right) \tag{D.12}$$

Following the definition of the acceleration factor in equation D.7 the acceleration factor for a sawtooth shaped stress signal can be written as

$$a_{\sigma_d} = \left(\frac{\sqrt{3}\tau_0}{2\bar{\tau}_d(\sqrt{3}+\mu)}\right) \cdot \left(\exp\left(\frac{\bar{\tau}_d(\sqrt{3}+\mu)}{\sqrt{3}\tau_0}\right) - \exp\left(-\frac{\bar{\tau}_d(\sqrt{3}+\mu)}{\sqrt{3}\tau_0}\right)\right) \tag{D.13}$$

The equation shows resemblance with a hyperbolic sine and can therefor be reduced to

$$a_{\sigma_d} = \left(\frac{\sqrt{3}\tau_0}{\bar{\tau}_d(\sqrt{3}+\mu)}\right) \cdot \sinh\left(\frac{\bar{\tau}_d(\sqrt{3}+\mu)}{\sqrt{3}\tau_0}\right) \tag{D.14}$$

Appendix E

Retardation time spectrum

The retardation time spectrum is obtained from a fitting of a measured compliance curve using a Kelvin-Voigt model. The relaxation spectrum is obtained from fitting of a conversion of the linear compliance curve using a Maxwell model. The retardation time and relaxation time spectrum are adapted from the work of Klompen et al. [9].

i	τ_i $[s]$	D_i $[GPa^{-1}]$
1	$3.14 \cdot 10^3$	0.00878
2	$3.59 \cdot 10^4$	0.00485
3	$4.10 \cdot 10^5$	0.00524
4	$4.68 \cdot 10^6$	0.00470
5	$5.34 \cdot 10^7$	0.01283
6	$6.10 \cdot 10^8$	0.01634
7	$6.97 \cdot 10^9$	0.02057
8	$7.96 \cdot 10^{10}$	0.02559
9	$9.09 \cdot 10^{11}$	0.03076
10	$1.04 \cdot 10^{13}$	0.04076
11	$1.19 \cdot 10^{14}$	0.04839
12	$1.35 \cdot 10^{15}$	0.06606
13	$1.55 \cdot 10^{16}$	0.09883
14	$1.77 \cdot 10^{17}$	0.04723
D_0	$= 0.419$	$[GPa^{-1}]$
η_0	$= 2.74 \cdot 10^{21}$	$[MPa\ s]$

Table E.1: Retardation times determined for Lexan 161R at 23°C, with a S_a-value of 28.3.

i	τ_i $[s]$	E_i $[MPa]$
1	$1.08 \cdot 10^3$	25.2
2	$1.12 \cdot 10^4$	42.1
3	$1.17 \cdot 10^5$	22.3
4	$1.21 \cdot 10^6$	23.8
5	$1.26 \cdot 10^7$	36.7
6	$1.31 \cdot 10^8$	70.5
7	$1.36 \cdot 10^9$	76.1
8	$1.41 \cdot 10^{10}$	90.5
9	$1.47 \cdot 10^{11}$	98.5
10	$1.52 \cdot 10^{12}$	109.5
11	$1.58 \cdot 10^{13}$	123.0
12	$1.64 \cdot 10^{14}$	128.4
13	$1.71 \cdot 10^{15}$	141.5
14	$1.23 \cdot 10^{16}$	33.8
15	$1.57 \cdot 10^{16}$	124.7
16	$2.17 \cdot 10^{18}$	1173.0
17	$2.77 \cdot 10^{18}$	71.0

Table E.2: relaxation times determined for Lexan 161R at 23°C, with a S_a-value of 28.3.